bioRxiv preprint doi: https://doi.org/10.1101/2021.12.03.471189; this version posted December 9, 2021. The copyright holder for this preprint (which was not certified by peer review) is the author/funder. All rights reserved. No reuse allowed without permission.

Glutamine deficiency in solid tumors confers resistance to ribosomal RNA synthesis inhibitors

Melvin Pan[1], Christiane Zorbas[2], Maki Sugaya[1], Kensuke Ishiguro[3,4], Miki Kato[1], Miyuki Nishida[1], Hai-Feng Zhang[5,6], Marco M Candeias[7], Akimitsu Okamoto[3], Takamasa Ishikawa[8], Tomoyoshi Soga[8], Hiroyuki Aburatani[9], Juro Sakai[10], Yoshihiro Matsumura[10], Tsutomu Suzuki[3], Christopher G. Proud[11], Denis L. J. Lafontaine[2], and Tsuyoshi Osawa[1*]

[1]Division of Integrative Nutriomics and Oncology, RCAST, The University of Tokyo, 4-6-1 Komaba, Meguro-ku, Tokyo 153-8904, Japan

[2]RNA Molecular Biology, Fonds de la Recherche Scientifique (F.R.S.-FNRS), Université Libre de Bruxelles (ULB), Biopark campus, 6041 Gosselies, Belgium

[3]Department of Chemistry and Biotechnology, Graduate School of Engineering, University of Tokyo, Tokyo 113-8656, Japan

[4]RIKEN Center for Biosystems Dynamics Research, 1-7-22 Suehiro-cho, Tsurumi-ku, Yokohama, Kanagawa 230-0045, Japan

[5]Department of Molecular Oncology, BC Cancer, Vancouver V5Z 1L3, Canada

[6]Department of Pathology and Laboratory Medicine, University of British Columbia, Vancouver V6T 2B5, Canada

[7]Molecular and RNA Cancer Unit, Graduate School of Medicine, Kyoto University,

bioRxiv preprint doi: https://doi.org/10.1101/2021.12.03.471189; this version posted December 9, 2021. The copyright holder for this preprint (which was not certified by peer review) is the author/funder. All rights reserved. No reuse allowed without permission.

Kyoto, Japan

[8]Institute for Advanced Biosciences, Keio University, Tsuruoka 997-0052, Japan

[9]Genome Science Division, RCAST, The University of Tokyo, 4-6-1 Komaba, Meguro-ku, Tokyo 153-8904, Japan

[10]Division of Metabolic Medicine, RCAST, The University of Tokyo, 4-6-1 Komaba, Meguro-ku, Tokyo 153-8904, Japan

[11]Lifelong Health, South Australian Health & Medical Research Institute, Adelaide, SA, 5000, Australia; School of Biomedical Sciences, University of Adelaide, Adelaide, SA, 5005, Australia

*To whom correspondence should be addressed, e-mail: osawa@lsbm.org

bioRxiv preprint doi: https://doi.org/10.1101/2021.12.03.471189; this version posted December 9, 2021. The copyright holder for this preprint (which was not certified by peer review) is the author/funder. All rights reserved. No reuse allowed without permission.

Summary

Ribosome biogenesis involves the processing of precursor ribosomal RNAs (pre-rRNAs) and sequential assembly with ribosomal proteins. Here we report that nutrient deprivation severely impairs pre-rRNA processing and leads to the accumulation of unprocessed rRNAs. Upon nutrient restoration, the accumulated pre-rRNAs are processed into mature rRNAs that are utilized for ribosome biogenesis. Failure to accumulate pre-rRNAs under nutrient deprivation leads to perturbed ribosome assembly during nutrient restoration and subsequent apoptosis via uL5/uL18-mediated activation of p53. Restoration of glutamine alone activates p53 by triggering uL5/uL18 translation. Induction of uL5/uL18 protein synthesis by glutamine was dependent on the translation factor eukaryotic elongation factor 2 (eEF2), which was in turn dependent on Raf/MEK/ERK signalling. Depriving cells of glutamine prevents the activation of p53 by rRNA synthesis inhibitors. Our data reveals a mechanism that cancer cells can exploit to suppress p53-mediated apoptosis during fluctuations in environmental nutrient availability.

Keywords

Metabolic adaptation, p53, tumor microenvironment, Ribosome, Ribosomal RNA synthesis and processing, nucleolar surveillance, RNA Polymerase I, CX-5461

bioRxiv preprint doi: https://doi.org/10.1101/2021.12.03.471189; this version posted December 9, 2021. The copyright holder for this preprint (which was not certified by peer review) is the author/funder. All rights reserved. No reuse allowed without permission.

Introduction

Solid tumors outstrip their blood supply and develop tissue microenvironments that are depleted of oxygen and nutrients[1,2]. Such microenvironments are characterized by chronic hypoxia and are typically located more than 180 μm away from blood vessels[3,4]. Another type of hypoxia— known as 'cycling hypoxia' — arises from transient shutdown of immature vasculature and can lead to 'reoxygenation injury', where increased free radical synthesis causes oxidative stress and tissue damage[5,6]. Along with hypoxia, an unstable blood supply also causes substantial fluctuations in nutrient availability in the tumor microenvironment[7]. Nutrient deprivation severely inhibits tumor cell proliferation but selects for aggressive cells that display increased angiogenic and metastatic ability[8,9].

In order to preserve energy balance during metabolic stress, tumor cells evolve adaptive mechanisms to attenuate ATP-costly processes under nutrient deprivation[10–12]. These adaptations involve the inhibition of protein synthesis, which is the most energy consuming process in the cell[12]. For instance, the eukaryotic elongation factor 2 kinase (eEF2K) is activated under nutrient restriction and inhibits the translation elongation factor eEF2, thereby suppressing overall protein synthesis and promoting cell survival under nutrient depletion[2]. Metabolic stress inhibits mammalian target of rapamycin complex 1 (mTORC1)[13]. This impairs mRNA translation initiation by activation of the eIF4E-binding protein 1 (4E-BP1), which inhibits the cap-binding translation initiation factor eIF4E[13]. Nutrient stress also triggers the integrated stress response (ISR), which leads to the inactivation of the translation factor eIF2α, thereby inhibiting translation initiation and promoting the synthesis of stress-adaptive proteins including ATF4[14]. Another critical adaptation is

bioRxiv preprint doi: https://doi.org/10.1101/2021.12.03.471189; this version posted December 9, 2021. The copyright holder for this preprint (which was not certified by peer review) is the author/funder. All rights reserved. No reuse allowed without permission.

the suppression of rRNA synthesis by RNA Polymerase I (Pol I), which comprises up to 60% of total cellular transcription[15,16]. mTORC1 and AMP-activated protein kinase (AMPK) reciprocally regulate pre-rRNA biosynthesis by phosphorylating TIF-IA, the protein complex that anchors Pol I to the rDNA promoter[15,16]. While oncogenic adaptations to nutrient deprivation have been well characterized, it is unknown how starving tumor cells resume proliferative capacities upon nutrient restoration.

Ribosome biogenesis is a highly sophisticated pathway that requires the production of four rRNAs and eighty ribosomal proteins[17,18]. Hundreds of protein *trans*-acting factors and small nucleolar RNAs aid the assembly process[17,18]. The process starts in the nucleolus where Pol I synthesizes a long polycistronic pre-rRNA that undergoes rapid folding, modification, processing, and associations with ribosomal proteins[19,20]. In unstressed cells, the tumor suppressor p53 is maintained at low levels by constitutive proteasomal degradation promoted by MDM2 (HDM2 in humans, henceforth denoted MDM2)[21]. When ribosome biogenesis is compromised, ribosomal components freely accumulate, including the ribosomal proteins uL5 (formerly known as RPL11) and uL18 (RPL5), which, together with the 5S rRNA, form a stable trimeric complex that binds and inhibits MDM2, leading to p53 stabilization and subsequent p53-mediated cell cycle arrest or apoptosis[22–24].

Given the importance of ribosome biogenesis in cancer cell growth, highly potent first-in-class Pol I inhibitors— such as CX-5461 and BMH-21 — have been developed to block rRNA synthesis and stabilize p53[25,26]. These inhibitors have the advantage of stabilizing p53 without inducing severe DNA damage, which is beneficial over mainstay genotoxic chemotherapies. Surprisingly, despite the importance of ribosome biogenesis to all cell types, single agent therapy with

bioRxiv preprint doi: https://doi.org/10.1101/2021.12.03.471189; this version posted December 9, 2021. The copyright holder for this preprint (which was not certified by peer review) is the author/funder. All rights reserved. No reuse allowed without permission.

CX-5461 has proven more effective against p53 wild type hematological malignancies than against p53 wild type solid tumors[25,27–29]. Notably, CX-5461 has been shown to possess antitumor activity against select solid tumor cell lines[30]. However, given the lack of data demonstrating *in vivo* on-target drug activity (pre-rRNA depletion, p53 stabilization), it is not entirely clear whether the antitumor activity is due to on-target or secondary effects.

Here, we report that nutrient deprivation severely impairs pre-rRNA processing and causes the accumulation of unprocessed rRNAs. Upon nutrient refeeding, protein synthesis resumes and newly synthesized ribosomal proteins (including uL5/uL18) associate with stored pre-rRNAs for ribosome assembly. Failure to accumulate pre-rRNAs under nutrient starvation leads to cell lethal p53 stabilization, which is caused by uL5/uL18-mediated inhibition of MDM2. We also show that the activation of p53 by uL5/uL18 is dependent on glutamine availability. Glutamine mediates the production of unassembled uL5/uL18 by activating Ras/Raf/MEK/ERK signalling, which suppresses eEF2K to allow global eEF2-mediated translation. Our study identifies pre-rRNA accumulation as a mechanism by which cells use to stay alive during fluctuations in environmental nutrient availability. Finally, we show that glutamine deprivation prevents the activation of p53 by rRNA synthesis inhibitors, strongly suggesting that glutamine-deficient solid tumors display inherent resistance to small molecules that target Pol I.

bioRxiv preprint doi: https://doi.org/10.1101/2021.12.03.471189; this version posted December 9, 2021. The copyright holder for this preprint (which was not certified by peer review) is the author/funder. All rights reserved. No reuse allowed without permission.

Results

Nutrient deprivation upregulates pre-rRNA expression

We first sought to understand how nutrient stress affects the rate of pre-rRNA synthesis by Pol I. We used the 5-fluorouridine (**5FU**) labelling assay to measure nascent pre-rRNA synthesis (see "Methods"). 5FU is a nucleoside analog that is incorporated into nascent RNAs, however, as the majority of newly synthesized RNA is pre-rRNA, 5FU labelling mainly occurs in the nucleolus (**Supplementary Fig. 1a**). Of note, this assay measures the rate of pre-rRNA synthesis (*i.e.* Pol I activity) rather than total pre-rRNA expression. To study nutrient stress, a panel of cell lines (colorectal HCT116, melanoma A375, lung adenocarcinoma A549, osteosarcoma U2OS, gastric MKN45) were cultured in medium lacking glucose, amino acids, and serum for 24 h. 5FU incorporation was significantly suppressed by nutrient deprivation (**ND**) in all cell lines tested (**Fig. 1a**). Thus, Pol I-mediated pre-rRNA synthesis is abrogated by metabolic stress.

We next tested the effect of ND on the expression of each pre-rRNA species (**Fig. 1b**). HCT116 cells were subjected to ND for 24 h and pre-rRNA expression was analyzed by northern blotting. The Pol I inhibitor CX-5461 was used as a positive control for the inhibition of pre-rRNA synthesis. As expected, CX-5461 swiftly depleted the expression of all pre-rRNA intermediates within 2 h (**Fig. 1c**). This acute effect is due to the short half-lives of the pre-rRNAs (approximately 30 minutes), which is in turn caused by rapid processing[30]. Surprisingly, despite the inhibitory effect of ND on pre-rRNA synthesis, the expression of large precursors (47S, 45S) did not decrease after 24 h ND (**Fig. 1c**). ND also induced the robust upregulation of the downstream 30S species by approximately two-fold (**Fig. 1c**). Other precursors

bioRxiv preprint doi: https://doi.org/10.1101/2021.12.03.471189; this version posted December 9, 2021. The copyright holder for this preprint (which was not certified by peer review) is the author/funder. All rights reserved. No reuse allowed without permission.

(21S, 18-SE) were slightly downregulated after 24 h of ND but were not decreased to the extent observed in CX-5461 treated cells (**Fig. 1c, Supplementary Fig. 1b**). Similarly, in mouse 3T3-L1 fibroblasts, ND did not affect 47S/45S levels and upregulated the 34S intermediate (equivalent to human 30S) (**Fig. 1d**). Taken together, these results show that suppressed pre-rRNA synthesis under ND does not lead to decreased pre-rRNA expression.

We next used qRT-PCR to quantify the effect of ND on pre-rRNA levels. Given that the 30S intermediate is upregulated by ND (**Fig. 1c**), we selected primers that measure the total abundance of the 47S, 45S, and 30S precursors. These primers bind across a cleavage site of the 5'-external transcribed sequence (5'ETS) of the pre-rRNA (**Supplementary Fig. 1d**). CX-5461 significantly decreased pre-rRNA expression (**Fig. 1e**). In contrast, 24 h ND significantly upregulated pre-rRNA levels in HCT116, A549, U2OS, and MKN45 cells (**Fig. 1f**).

Pre-rRNA processing is impaired under ND

We hypothesized that upregulated pre-rRNA levels under ND is a direct consequence of impaired pre-rRNA processing. We used the L-(methyl-^{3}H)-methionine metabolic labelling assay to assess pre-rRNA processing[31]. Control and ND HCT116 cells were pulsed with L-(methyl-^{3}H)-methionine for 30 min and then chased with excess cold methionine (**Fig. 2a**). The maturation of L-(methyl-^{3}H)-methionine labelled pre-rRNAs was tracked over 4 hours. In control cells, the expression of large precursors (47S, 45S) and downstream intermediates (32S, 30S) quickly decreased over time, indicating that these precursors were metabolized into mature 18S/28S rRNAs (**Fig. 2a**). In contrast, ND caused the robust

bioRxiv preprint doi: https://doi.org/10.1101/2021.12.03.471189; this version posted December 9, 2021. The copyright holder for this preprint (which was not certified by peer review) is the author/funder. All rights reserved. No reuse allowed without permission.

accumulation of the 47S, 45S, 32S, and 30S precursors (**Fig. 2a**), demonstrating that these intermediates did not mature to 18S/28S rRNAs. Accordingly, the production of 18S and 28S rRNAs was strongly impaired under ND (**Fig. 2b**). Remarkably, adding back the non-essential amino acid glutamine to starved cells fully rescued 18S and 28S rRNA production (**Fig. 2b**). This indicates that unprocessed rRNAs that accumulate under ND are utilized for ribosome biogenesis during nutrient restoration.

To rigorously confirm that ND slows pre-rRNA processing, we measured the pre-rRNA half-life using qRT-PCR and the 5'ETS primers (**Supplementary Fig. 1d**). Transcription was blocked in control and ND HCT116 cells using actinomycin D (20 μM), and pre-rRNA expression was monitored over 1 h (see "Methods"). In control HCT116 cells, the pre-rRNA half-life was approximately 28 min, while cells subjected to ND displayed a significantly longer half-life of 78 min (**Fig. 2c**). Similarly, ND increased the pre-rRNA half-life by at least two-fold in A375, A549, U2OS, and MKN45 cells (**Fig. 2d**).

Solid tumors are insufficiently vascularized with microenvironments that are strongly deprived of nutrients[7]. We therefore sought to estimate the half-life of pre-rRNAs *in vivo*. To investigate this, we injected a highly concentrated solution of actinomycin D (1.33 mM) directly into HCT116 tumors to acutely halt transcription. Inhibition of Pol I transcription by actinomycin D is known to cause the translocation of nucleolar proteins to the nucleoplasm, a process known as nucleolar disruption[33,34]. Thus, we first confirmed the inhibition of Pol I by assessing the localization of nucleolin, a classical nucleolar marker. Indeed, many intact nucleolin-positive nucleoli were observed in control tumors, but nucleolin staining was found in the cytoplasm in tumors injected with actinomycin D (**Supplementary**

bioRxiv preprint doi: https://doi.org/10.1101/2021.12.03.471189; this version posted December 9, 2021. The copyright holder for this preprint (which was not certified by peer review) is the author/funder. All rights reserved. No reuse allowed without permission.

Fig. 2a). Next, to assess the stability of pre-rRNAs *in vivo*, HCT116 tumors were intratumorally injected with actinomycin D and tissues were collected for RNA extraction and qRT-PCR analysis. Tumoral pre-rRNAs displayed a half-life of approximately 3.8 h (**Fig. 2e**). Further, actinomycin D had no significant effect on 18S and 28S expression (**Fig. 2f**). Next, since it has been shown that the cores of solid tumors are more severely depleted of nutrients compared to the periphery[35], we reasoned that core tumor cells would display slower pre-rRNA processing kinetics than cells in the periphery. To test this, large HCT116 tumors (>1000mm^3) were injected with actinomycin D and peripheral and core tissues were dissected to differentiate tumor cells under high or low nutrient conditions, respectively (**Fig. 2g**)[35]. Core tissues expressed higher levels of HIF-1α, consistent with the notion that core regions of solid tumors are hypoxic (**Fig. 2h**). Furthermore, metabolomic analysis showed that core tissues had significantly lower levels of several metabolites including glutamine, arginine, serine, and histidine (**Supplementary Fig. 2e**). Finally, in line with our hypothesis, peripheral pre-rRNAs exhibited a half-life of 3.5 h while core pre-rRNAs displayed a significantly longer half-life of 8.3 h (**Fig. 2i**).

Pre-rRNA accumulation is an adaptive response to nutrient restoration

Since we observed that pre-rRNAs that accumulate under ND are utilized for ribosome biogenesis during nutrient (glutamine) feedback (**Fig. 2b**), we hypothesized that accumulated pre-rRNAs may facilitate the resumption of ribosome assembly during nutrient recovery. To address this, we tested whether preventing pre-rRNA accumulation under ND leads to perturbed ribosome assembly during metabolic recovery. First, to prevent pre-rRNA accumulation, HCT116 or A375 cells were

bioRxiv preprint doi: https://doi.org/10.1101/2021.12.03.471189; this version posted December 9, 2021. The copyright holder for this preprint (which was not certified by peer review) is the author/funder. All rights reserved. No reuse allowed without permission.

placed under ND with co-treatment of vehicle, CX-5461, or BMH-21 (a second Pol I inhibitor). CX-5461 and BMH-21 blocked the accumulation of pre-rRNAs under ND (**Fig. 3a**). Notably, ND (24 h) alone caused approximately 50% cell death, but this was not exacerbated by CX-5461 or BMH-21 co-treatment (**Fig. 3b**). Herein, we refer to cells pre-treated with ND+CX-5461 or ND+BMH-21 as 'pre-rRNA-depleted cells'. Next, to assess the fidelity of ribosome assembly during metabolic recovery, we transferred pre-starved cells to drug-free nutrient-rich media for 8 h and assessed the expression of unassembled ribosomal proteins (**Fig. 3c, Methods**). Defects in ribosome biogenesis causes the accumulation of unassembled ribosomal proteins that have not been incorporated into mature ribosomes[36]. Thus, large ribosomes were removed from cell lysates using sucrose cushion ultracentrifugation and the resulting ribosome-free lysates were analyzed by western blotting (**Fig. 3d**). We focused on the expression of the key ribosomal proteins uL5 (formerly RPL11) and uL18 (RPL5) because these two proteins have been shown to specifically accumulate in the ribosome-free fraction upon impaired ribosome biogenesis[36]. Ribosome-free uL5/uL18 was undetectable in ND vehicle cells subjected to nutrient restoration (**NR**), indicating that newly translated uL5/uL18 were efficiently incorporated into ribosomes during metabolic recovery (**Fig. 3e**). In contrast, unassembled uL5/uL18 was expressed in pre-rRNA-depleted cells (ND+CX-5461) subjected to NR (**Fig. 3e**). This showed that these ribosomal proteins were not incorporated into ribosomes. Moreover, we observed that halting translation with cycloheximide (CHX) prevented the accumulation of unassembled uL5/uL18 (**Fig. 3e**). This is consistent with the proposed model that ongoing protein synthesis is required for the accumulation of unassembled uL5/uL18[36]. We further assessed

bioRxiv preprint doi: https://doi.org/10.1101/2021.12.03.471189; this version posted December 9, 2021. The copyright holder for this preprint (which was not certified by peer review) is the author/funder. All rights reserved. No reuse allowed without permission.

whether perturbed ribosome assembly was associated with nucleolar disruption. Indeed, nucleolin was found in the nucleoplasm of pre-rRNA-depleted cells exposed to NR, whereas the staining was confined to the nucleolus in control cells (**Supplementary Fig. 3a**).

To assess the consequence of impaired ribosome assembly, cells depleted of pre-rRNAs were exposed to prolonged NR (24 h) and cell recovery was initially assessed using light microscopy. Starved control (ND+Vehicle) HCT116 and A375 cells resumed proliferation after NR, as shown by increased confluence (**Fig. 3f**). In striking contrast, starved pre-rRNA-depleted HCT116 cells exposed to NR did not resume proliferation and also exhibited features of apoptosis such as reduced cell size and rounded morphology (**Fig. 3f**). Trypan blue exclusion assays revealed profound levels of cell death in pre-rRNA-depleted cells exposed to NR but not in control cells (**Fig. 3g**). The presence of cleaved caspase-3 and PARP indicated that NR-mediated cell death was apoptosis, detection of which was abrogated by the addition of the pan-caspase inhibitor zVAD-FMK (**Fig. 3h**). Furthermore, we observed that pre-rRNA-depleted cells resumed pre-rRNA synthesis upon NR (**Fig. 3i**). This indicates that the effects of CX-5461 and BMH-21 are reversible. Taken together, these results show that failure to accumulate pre-rRNAs under ND leads to perturbed ribosomal subunit assembly and apoptosis during NR.

Nucleolar surveillance drives NR-mediated apoptosis

When ribosome assembly is disturbed, unassembled uL5/uL18 accumulate and bind to MDM2 in an inhibitory manner, leading to the stabilization of p53 and activation of p53-dependent apoptosis[22–25,36–38]. This mode of cell death is known as

bioRxiv preprint doi: https://doi.org/10.1101/2021.12.03.471189; this version posted December 9, 2021. The copyright holder for this preprint (which was not certified by peer review) is the author/funder. All rights reserved. No reuse allowed without permission.

the nucleolar surveillance pathway. Thus, we hypothesized that the p53-driven nucleolar surveillance pathway was the primary mechanism by which NR induces apoptosis in cells depleted of pre-rRNAs. To address this, we assessed the expression of p53 and found that pre-rRNA-depleted cells (ND+CX-5461/ND+BMH-21) exposed to NR accumulated high levels of p53, whereas starved vehicle (ND+Vehicle) cells did not accumulate p53 (**Fig. 4a**). Similar results were observed in A375 cells (**Supplementary Fig. 3b**). We next immunoprecipitated MDM2 to assess the expression of associated uL5/uL18. MDM2 was undetectable in control ND cells, but was upregulated in pre-rRNA-depleted cells exposed to NR (**Fig. 4b**). This upregulation is due to MDM2 being a downstream transcriptional target of p53. Importantly, in cells depleted of pre-rRNAs, immunoprecipitation of MDM2 showed high levels of associated uL5/uL18 (**Fig. 4b**).

We next tested whether compromising the nucleolar surveillance pathway could alleviate NR-mediated apoptosis. We therefore performed a double knockdown of uL5 and uL18 using two independent sets of siRNAs and assessed the activation of p53 and apoptotic markers. Dual depletion of uL5 and uL18 completely blocked the stabilization of p53 and greatly reduced PARP and Caspase 3 cleavage (**Fig. 4c**). Likewise, dual knockdown of uL5 and uL18 also decreased NR-mediated activation of p53 in A375 and A549 cells (**Supplementary Fig. 3c**). Independently silencing uL5 or uL18 alone also strongly inhibited p53 (**Supplementary Fig. 3d**). Further support for the role of p53 in NR-mediated apoptosis was obtained using p53 wildtype or knockout HCT116 cells. Pre-rRNA-depleted HCT116 p53 -/- cells exposed to NR exhibited lower levels of apoptosis compared to wildtype counterparts as shown by decreased activation of apoptotic markers and Annexin V staining (**Fig. 4d,**

bioRxiv preprint doi: https://doi.org/10.1101/2021.12.03.471189; this version posted December 9, 2021. The copyright holder for this preprint (which was not certified by peer review) is the author/funder. All rights reserved. No reuse allowed without permission.

4e). Finally, siRNAs targeting p53 or PUMA (the downstream effector of p53) also strongly alleviated NR-induced apoptosis in HCT116 and A375 cells (**Supplementary Fig. 4a, 4b, 4c, 5a**).

Taken together, these data show that cancer cells accumulate unprocessed rRNAs under starvation in order to escape the p53-driven nucleolar surveillance pathway during nutrient refeeding (**Fig. 4f**). Pre-rRNAs that accumulate during starvation are utilized for ribosome biogenesis upon metabolic recovery (**Fig. 4f**). Failure to accumulate pre-rRNAs under starvation leads to dysfunctional ribosome assembly during nutrient recovery, which causes unassembled uL5/uL18 to bind to MDM2 and trigger cell lethal p53 activation (**Fig. 4f**).

Glutamine metabolically activates p53 by inducing uL5/uL18 translation

The activation of p53 through the nucleolar surveillance pathway requires ongoing de novo protein synthesis of uL5 and uL18[36,39]. Thus, the activation of p53 serves as a proxy marker for ongoing uL5/uL18 mRNA translation. Given this, we found that refeeding glutamine alone was sufficient to rescue p53 in pre-rRNA-depleted HCT116 and A375 cells (**Fig. 5a, Supplementary Fig. 5b**). In contrast, restoration of leucine, tyrosine, and methionine did not stabilize p53 (**Supplementary Fig. 5c**). In addition, dual knockdown of uL5/uL18 inhibited the stabilization of p53 by glutamine (**Supplementary Fig. 5d**). These results indicate that glutamine metabolically activates p53 in pre-rRNA-depleted cells by inducing uL5/uL18 protein synthesis. Finally, we found that glutamine also reactivated mTORC1, as shown by the increase in the phosphorylation of S6K (Thr 389), a known mTORC1 substrate (**Fig. 5a**). This finding is consistent with the role of glutamine in activating mTORC1[40,41]. This

bioRxiv preprint doi: https://doi.org/10.1101/2021.12.03.471189; this version posted December 9, 2021. The copyright holder for this preprint (which was not certified by peer review) is the author/funder. All rights reserved. No reuse allowed without permission.

prompted us to examine whether mTORC1 is required for the metabolic stabilization of p53. To test this, we exposed pre-rRNA-depleted cells to glutamine in the presence of rapamycin or Torin1, two highly potent and specific mTORC1 inhibitors. However, contrary to our hypothesis, rapamycin or Torin1 had no effect on the metabolic accumulation of p53 (**Fig. 5b**).

We therefore wondered whether other pathways that modulate protein synthesis, such as the Ras/Raf/MEK/ERK signaling cascade, might regulate glutamine-mediated synthesis of uL5/uL18. Indeed, we observed that glutamine restoration rescued MEK and ERK phosphorylation in pre-rRNA-depleted A375 cells (**Fig. 5c**). To test whether the metabolic stabilization of p53 is dependent on Raf/MEK/ERK signalling, we refed pre-rRNA-depleted cells with glutamine in combination with the pan-Raf inhibitors LY3009210 (400 nM) or AZ628 (500 nM). Strikingly, both pan-Raf inhibitors blocked the activation of p53 by glutamine (**Fig. 5d**). As expected, LY3009210 or AZ628 strongly decreased ERK and MEK phosphorylation (**Fig. 5d**).

We next sought to understand the potential regulatory effects of Raf/MEK/ERK signalling on uL5/uL18 translation. Given that mTORC1 primarily regulates translation initiation[42], and that mTORC1 suppression did not inhibit p53 (**Fig. 5b**), we reasoned that Raf/MEK/ERK might regulate uL5/uL18 via the elongation step of translation. Indeed, in unstressed cells, Raf/MEK/ERK facilitates mRNA translation by inhibiting eukaryotic elongation factor-2 kinase (eEF2K), a key negative regulator of translation elongation (**Fig. 5e**)[43,44]. Upon eEF2K inhibition, its downstream target eukaryotic elongation factor-2 (eEF2) remains in its active unphosphorylated form to mediate global translation elongation (**Fig. 5e**)[43,44]. Thus, we hypothesized that

bioRxiv preprint doi: https://doi.org/10.1101/2021.12.03.471189; this version posted December 9, 2021. The copyright holder for this preprint (which was not certified by peer review) is the author/funder. All rights reserved. No reuse allowed without permission.

uL5/uL18 translation is dependent on Raf/MEK/ERK-mediated activation of eEF2 (**Fig. 5e**). We therefore assayed levels of eEF2 phosphorylation; phosphorylated eEF2 (Thr56) being the inactivated form that leads to arrest of general protein synthesis[43,44]. Indeed, inhibition of Raf with LY3009210 or AZ628 robustly increased eEF2 phosphorylation in both starved control and pre-rRNA-depleted cells (**Fig. 5d**). Likewise, pharmacological inhibition of MEK (U0126, PD98059) or ERK (LY3214996, GDC-0994) similarly induced eEF2 phosphorylation and p53 inhibition (**Fig. 5f**). This was further observed in A375 cells, in which inhibition of Raf (LY3009210), MEK (U0126), or ERK (LY3214996) completely blocked p53 expression (**Fig. 5g**). Next, to assess the effect of Raf inhibition on uL5/uL18 mRNA translation, we measured the expression of translationally active polysome-bound mRNAs (see “Methods”). ND alone decreased the proportion of polysome-bound uL5/uL18 mRNAs (**Fig. 5h**). Importantly, glutamine restoration rescued uL5/uL18 mRNA translation, but was inhibited by co-incubation with LY3009210 (**Fig. 5h**). Consistent with the role of eEF2 in general mRNA translation[43,44], a similar effect was observed with uL23 and S3 polysome-bound mRNAs (**Fig. 5h**).

Glutamine deprivation confers cancer cells resistance to RNA Pol I inhibitors by blocking the nucleolar surveillance pathway

Since glutamine restoration stabilized p53 in pre-rRNA-depleted cells (**Fig. 5a**), we next tested the effect of glutamine deprivation on the activation of p53 by CX-5461. Strikingly, glutamine deprivation blocked the activation of p53 by CX-5461, while the withdrawal of glucose or other amino acids had no effect (**Fig. 6a**). Suppression of p53 transcriptional activity under glutamine deprivation was confirmed by measuring

bioRxiv preprint doi: https://doi.org/10.1101/2021.12.03.471189; this version posted December 9, 2021. The copyright holder for this preprint (which was not certified by peer review) is the author/funder. All rights reserved. No reuse allowed without permission.

p21 mRNA (**Supplementary Fig. 6a**). Glutamine deprivation inhibited the activation of p53 by BMH-21 and two other Pol I inhibitors, CX-3543 and actinomycin D (**Fig. 6b**). Glutamine deprivation also inhibited p53 in A375, A549, U2OS, LNCaP, and MKN45 cells (**Fig. 6c**), and conferred resistance to CX-5461 in HCT116 cells (**Fig. 6d**) as well as LNCaP and MKN45 cells (**Supplementary Fig. 6b**). Glucose deprivation, which does not inhibit p53, did not confer resistance to CX-5461 (**Fig. 6d**). Overexpression of p53 under glutamine deprivation rescued the growth suppressive effects of CX-5461 (**Supplementary Fig. 6c**). In addition, rescuing p53 with the non-genotoxic MDM2 inhibitor AMG 232 also inhibited the viability of glutamine-deprived cells (**Supplementary Fig. 6d**).

Solid tumors contain low levels of glutamine due to rapid consumption by tumor cells[35]. Thus, we predicted that CX-5461 would fail to stabilize p53 *in vivo*. Indeed, p53 was suppressed under 0.4 mM glutamine (**Fig. 6e**), which is approximately the concentration of glutamine found in tumor xenografts[35]. We selected HCT116 as our model cell line, since CX-5461 has been shown to potently inhibit HCT116 *in vitro* cell proliferation at an IC50 167 nM[30]. Oral gavage of CX-5461 at the highest long-term tolerable dose (50 mg/kg) failed to significantly inhibit tumor growth (**Fig. 6f**). We used AMG 232 as a positive control for p53-mediated tumor suppression. Oral gavage of AMG 232 (50 mg/kg) at the same dose and schedule as CX-5461 significantly suppressed HCT116 tumor growth (**Fig. 6f**). Furthermore, IP injection of CX-5461 up to 200 mg/kg to HCT116 tumors failed to activate p53 while AMG 232 (50 mg/kg) robustly induced p53 (**Fig. 6g**). Similarly, AMG 232 but not CX-5461 stabilized p53 in A375 tumors (**Fig. 6h**). These results indicate that tumoral glutamine

bioRxiv preprint doi: https://doi.org/10.1101/2021.12.03.471189; this version posted December 9, 2021. The copyright holder for this preprint (which was not certified by peer review) is the author/funder. All rights reserved. No reuse allowed without permission.

deficiency hampers the antitumor activity of Pol I inhibitors by blocking the p53-dependent nucleolar surveillance pathway.

Discussion

Unstable vasculature in solid tumors leads to the development of tissue microenvironments that fluctuate in nutrient availability[7]. Tumor cells residing in such environments adapt to nutrient depletion by suppressing processes that heavily utilize ATP such as ribosome biogenesis[10–12], but how cells recover during nutrient restoration remains to be elucidated. Here, we report that metabolically stressed mammalian cells accumulate unprocessed rRNAs in order to escape nucleolar surveillance upon nutrient stress termination. We first observed that ND inhibits pre-rRNA processing, leading to the accumulation of pre-rRNA intermediates in nutrient starved cells. Upon nutrient restoration, recovering cells resume ribosome biogenesis and pre-rRNAs accumulated during stress are converted into mature rRNAs. Cells that fail to accumulate pre-rRNAs under ND undergo cell-lethal p53 activation during nutrient refeeding. Mechanistically, p53 is activated by unassembled uL5/uL18 binding and inhibiting MDM2. Our data shows that pre-rRNA accumulation during nutrient deprivation is a stress adaptation that restrains the MDM2-binding activity of uL5 and uL18 during fluctuations in nutrient availability.

We further identified that the activation of p53 through the uL5/uL18-dependent nucleolar surveillance pathway is dependent on exogenous glutamine. In pre-starved cells depleted of pre-rRNAs, refeeding glutamine was sufficient to stabilize p53, compatible with rescue of uL5/uL18 translation. Surprisingly, despite the known importance of mTORC1 in the translational control of 5'TOP mRNAs (that encode

bioRxiv preprint doi: https://doi.org/10.1101/2021.12.03.471189; this version posted December 9, 2021. The copyright holder for this preprint (which was not certified by peer review) is the author/funder. All rights reserved. No reuse allowed without permission.

ribosomal proteins including uL5 and uL18)[45,46], rapamycin or Torin1 treatment did not affect the stabilization of p53 by glutamine. Since the accumulation of p53 protein is a marker of uL5 and uL18 synthesis[36,39], this observation suggested that uL5/uL18 translation was not solely dependent on mTORC1. Rather, we found that pharmacologically inhibiting Raf/MEK/ERK completely blocked the accumulation of p53. Raf/MEK/ERK inhibition appeared to arrest the synthesis of uL5 and uL18 by inactivating eEF2. Altogether, these results suggest that glutamine-induced synthesis of uL5 and uL18 is facilitated by the Ras/Raf/MEK/ERK-eEF2K-eEF2 axis.

Finally, we found that glutamine deprivation confers resistance to CX-5461 by blocking the stabilization of p53. This finding was recapitulated in the low glutamine tumor microenvironment, where CX-5461 failed to stabilize p53 *in vivo* and consequently showed little inhibitory effect on HCT116 tumor growth. In line with our findings, another study observed that p53 wild-type HCT116 tumors are highly resistant to CX-5461[47]. This is despite another study demonstrating that HCT116 cells are remarkably sensitive to CX-5461 *in vitro*[30]. Thus, these results indicate that CX-5461 may display limited therapeutic benefit to solid tumors due to tumoral glutamine deficiency. Altogether, our data shows that tumoral glutamine deficiency hampers the effectiveness of Pol I inhibitors by blocking the nucleolar surveillance pathway. These findings offer an explanation as to why the efficacy of CX-5461 is not associated with p53 wild-type status in solid tumor types. Further, these results may explain why CX-5461 is highly effective against blood cancers[25,27–29], in which severe pathological nutrient deprivation does not occur. Indeed, plasma glutamine concentrations are approximately 0.8 mM[48], which is twice higher than the concentration at which p53 was found to be inhibited in this study (**Fig. 4e**). Further,

bioRxiv preprint doi: https://doi.org/10.1101/2021.12.03.471189; this version posted December 9, 2021. The copyright holder for this preprint (which was not certified by peer review) is the author/funder. All rights reserved. No reuse allowed without permission.

since the rate of ribosome biogenesis is dependent on nutrient availability, this implies that cells of hematological malignancies possess higher rates of ribosome biogenesis than cells of solid tumors and are therefore more vulnerable to Pol I inhibitors.

In summary, our study unveils a stress adaptive program that suppresses p53 during fluctuations in nutrient availability. Accumulation of unprocessed rRNAs emerges as a critical survival mechanism that is exploited by starving tumor cells to complete metabolic recovery during nutrient restoration. Further, solid tumors that are inherently depleted of glutamine do not accumulate p53 in response to Pol I inhibitors, highlighting how the metabolic landscape of the tumor microenvironment can deeply influence the therapeutic response to nucleolar function disruptors.

bioRxiv preprint doi: https://doi.org/10.1101/2021.12.03.471189; this version posted December 9, 2021. The copyright holder for this preprint (which was not certified by peer review) is the author/funder. All rights reserved. No reuse allowed without permission.

Materials and methods

Cell lines, Reagents, and siRNA transfections

HCT116, A375, A549, U2OS, and MKN45, cells were purchased from the American Type Culture Collection (Manassas, VA, USA). HCT116 p53+/+ and p53−/− isogenic human colon cancer cells were kindly provided by Bert Vogelstein (Johns Hopkins University). HCT116, A375, A549, and U2OS cells were grown in Dulbecco's modified Eagle's medium (DMEM) (Nacalai Tesque, Kyoto, Japan), supplemented with 10% fetal bovine serum (FBS) (Thermo Fisher Scientific). MKN45 cells were maintained in RPMI (Nacalai Tesque, Kyoto, Japan), supplemented with 10% FBS. Cells were maintained at 37°C in a 5% CO_2 atmosphere in a humidified incubator. Nutrient deprivation medium was prepared to contain inorganic salts, i.e., 0.2 g/l $CaCl_2$ (anhydrous), 0.1 mg/l $Fe(NO_3)_3$/9H2O, 0.4 g/l KCl, 97.67 mg/l $MgSO_4$ (anhydrous), 6.4 g/l NaCl, 3.7 g/l $NaHCO_3$, 0.125 g/l NaH_2PO_4/H_2O, and 15 mg/l Phenol Red, according to the composition of DMEM. Glutamine deprivation was performed with DMEM without glutamine (Fujifilm Wako 045-30285) supplemented with 10% FBS. Glutamine replete medium was made by adding 4 mM L-glutamine (Fujifilm Wako) to the glutamine deprivation medium. Glucose deprivation was performed with DMEM without glucose (Fujifilm Wako 042-32255) supplemented with 10% FBS. Glucose replete medium was made by adding 25 mM D-glucose (Fujifilm Wako) to the glucose deprivation medium. Tyrosine, leucine, and methionine medium were prepared according to the composition of DMEM (Nissui, Tokyo, Japan).

bioRxiv preprint doi: https://doi.org/10.1101/2021.12.03.471189; this version posted December 9, 2021. The copyright holder for this preprint (which was not certified by peer review) is the author/funder. All rights reserved. No reuse allowed without permission.

The compounds used in this study were obtained from: CX-5461 (MedChemExpress), AMG 232 (MedChemExpress), BMH-21 (Selleck), Camptothecin (Fujifilm Wako), Rapamycin (Fujifilm Wako), Torin1 (Fujifilm Wako), BEZ235 (Funakoshi), 5-Fluorouridine (TCI chemicals), Actinomycin D (Fujifilm Wako), zVAD-FMK (Fujifilm Wako), LY3009120 (Selleck), AZ628 (Selleck), U0126 (Selleck), PD98059 (Selleck), LY-3214996 (Selleck), GDC-0994 (Selleck)

Cancer cells were transfected at ~30% confluency in 6-well plates with 5nM control or target siRNA using Lipofectamine RNAiMAX (Invitrogen) according to the instructions of the manufacturer. Control siRNA and siRNAs designed against p53, PUMA, RPL5 (uL18), and RPL11 (uL5) were obtained from Thermo Fisher Scientific.

Trypan Blue assays, MTT assays

For trypan blue exclusion assays, 6 x 10^5 cells (HCT116, A375, A549, U2OS) were seeded in 6-well plates and the percentage of cell death was determined after 24 h ND. Cell counting was performed with the TC20 Automated Cell Counter (Bio-Rad) according to the instructions of the manufacturer. After 24 h ND, the treatment medium was set aside, adherent cells were detached with 100 µL trypsin and suspended with 900 µL of the treatment media. 100 µL of the suspension was mixed with 100 µL trypan blue solution (Bio-Rad) and analyzed with the TC20 Cell Counter.

For MTT assays, 6-10 x 105 cancer cells were seeded in 6-well plates, and after treatment, the cell media was aspirated and replaced with medium containing MTT

bioRxiv preprint doi: https://doi.org/10.1101/2021.12.03.471189; this version posted December 9, 2021. The copyright holder for this preprint (which was not certified by peer review) is the author/funder. All rights reserved. No reuse allowed without permission.

(0.5 mg/mL) (Fujifilm Wako) for 3 h and lysed with DMSO. Absorbance was measured at 570 nm with a plate reader.

Western Blotting

Cells were lysed with RIPA buffer containing a protease inhibitor cocktail (P8340 Sigma), phosphatase inhibitors (P0044 and P5726 Sigma), and 1 mM PMSF. Protein quantification was performed using BCA kit (Pierce). Cell lysates were applied to a 10% polyacrylamide gel and transferred to a nitrocellulose membrane (Thermo Fisher Scientific). The membrane was incubated with antibodies that target p53 (1:1000, Calbiochem), b-actin (1:1000, Sigma-Aldrich), phospho-S6K (T389) (1:1000, Cell Signaling Technology), S6K (1:1000, Cell Signaling Technology), phospho-S6 (S235/236) (1:1000, Cell Signaling Technology), S6 (1:1000, Cell Signaling Technology), phospho-4E-BP1 (Thr37/46) (1:1000, Cell Signaling Technology), 4E-BP1 (1:1000, Cell Signaling Technology), HIF-1α (1:1000 Novus Biologicals), Cleaved PARP (1:1000, Cell Signaling Technology), Caspase 3 (1:1000, Cell Signaling Technology), Cleaved Caspase 3 (1:1000, Cell Signaling Technology), PUMA (1:1000, Cell Signaling Technology), RPL5 (1:1000, kindly provided by Dr. Siniša Volarević), RPL11 (1:1000, kindly provided by Dr. Siniša Volarević), phospho-MEK1/2 (Ser217/221) (1:500 Cell Signaling Technology), MEK1/2 (1:500 Cell Signaling Technology), phospho-ERK1/2 (Thr202/Tyr204) (1:500 Cell Signaling Technology), ERK1/2 (Thr202/Tyr204) (1:500 Cell Signaling Technology), phospho-eEF2 (Thr56) (1:1000 Cell Signaling Technology), eEF2 (1:1000 Cell Signaling Technology), eEF2K (1:1000 Cell Signaling Technology), followed by incubation with horseradish peroxidase-conjugated secondary antibodies (1:5000,

bioRxiv preprint doi: https://doi.org/10.1101/2021.12.03.471189; this version posted December 9, 2021. The copyright holder for this preprint (which was not certified by peer review) is the author/funder. All rights reserved. No reuse allowed without permission.

Sigma-Aldrich). Signals were detected using enhanced chemiluminescence detection reagents (Thermo Fisher Scientific) and images were acquired using a luminescent image analyzer (LAS3000, Fuji-Film, Japan).

Isolation of Ribosome-free fractions and Polysome-bound mRNA

Ribosome-free fractions were collected according to a previously used protocol[36]. Metabolically recovering (ND to NR) HCT116 cells (4 x 10^8) were washed in PBS containing 100 µg/mL cycloheximide twice. Total cell extracts were suspended in 2.5 mL polysome buffer (20 mM Tris, 10 Mm $MgCl_2$, 300 mM KCl, 10 mM dithiothreitol, 100 units/mL RNasin, 100 µg/mL cycloheximide, protease and phosphatase inhibitors, pH 7.4) and gently sheared 4x using a 26-gauge needle. Total cell extracts were centrifuged (20,000 g 30 min) to pellet cell debris. The resulting cell extracts were layered over a 20% sucrose cushion (polysome buffer + 20% w/v sucrose) and ultracentrifuged (Beckman Coulter TLA100.3 Fixed-Angle Rotor, 149,000 g 2 h). The supernatant containing the non-ribosomal fraction was later assessed using western blotting. To isolate polysome-bound mRNAs, cell extracts were layered over a 40% sucrose cushion (polysome buffer + 40% w/v sucrose) and the ribosomal pellet was collected for RNA extraction and qRT-PCR.

Northern Blotting

Northern Blotting was performed as previously reported[19].

RNA Isolation and quantitative RT-PCR

Total RNA was extracted from cells using the Isogen reagent (Nippon Gene, Toyama, Japan), converted to cDNA by using the Prime Script reverse transcriptase (Takara,

bioRxiv preprint doi: https://doi.org/10.1101/2021.12.03.471189; this version posted December 9, 2021. The copyright holder for this preprint (which was not certified by peer review) is the author/funder. All rights reserved. No reuse allowed without permission.

Shiga, Japan) as per the manufacturer's instructions, and used for quantitative real-time PCR amplification using SYBR Green (Takara). Target RNA expression was normalized to β2m mRNA. Quantification of the pre-rRNA half-life was performed according to a previous report[32]. Briefly, cells were treated to an excess concentration of actinomycin D (20 μM) that blocks transcription within 30 seconds[32], and pre-rRNA expression was tracked over 1 h.

The following primer sequences were used:

For pre-rRNA expression:

5′-CCGCGCTCTACCTTACCTACCT-3'(forward);

5′-GCATGGCTTAATCTTTGAGACAAG-3′(reverse).

For human p21:

5′-TGTCCGTCAGAACCCATGC-3′;

5′-AAAGTCGAAGTTCCATCGCTC-3′.

For human β2m:

5′-AGATGAGTATGCCTGCCGTG-3′;

5′-CATCCAATCCAAATGCGGCA-3′.

For uL5 (RPL11):

5′-AAAGGTGCGGGAGTATGAGTT-3′;

5′-TCCAGGCCGTAGATACCAATG-3′.

For uL18 (RPL5):

5′-GCTCGGAAACGCTTGGTGATA-3′;

5′-CCCTCTATACGGGCATAAGCAAT-3′.

For uL23 (RPL23):

bioRxiv preprint doi: https://doi.org/10.1101/2021.12.03.471189; this version posted December 9, 2021. The copyright holder for this preprint (which was not certified by peer review) is the author/funder. All rights reserved. No reuse allowed without permission.

5′-TCCTCTGGTGCGAAATTCCG-3′;

5′-CGTCCCTTGATCCCCTTCAC-3′.

For S3 (RPS3):

5′-AGAGGAAGTTTGTCGCTGATG-3′;

5′-GCACCTCAACTCCAGAGTAGC-3′.

Annexin V-PI Flow Cytometry

After treatment, cancer cells were trypsinized, centrifuged (1000 rpm, 5 min) and resuspended in 1X Binding buffer with Annexin V and propidium iodide (PI) with a Annexin V-FITC Apoptosis Detection Kit (Abcam), according to the instructions of the manufacturer. Cells were analyzed on a BAD FACSverse flow cytometry instrument.

5-Fluorouridine Metabolic Labelling and Microscopy

To measure pre-rRNA biosynthesis, cells were seeded at 50% confluence in 6-well plates containing round cover glasses (12CIR-1D; Thermo Fisher Scientific). After treatment, cells were incubated with 10 μM 5-Fluorouridine (5FU) (TCI chemicals) for 3 h, followed by fixation with methanol at -20°C for 30 min and blocking with milk (5% in PBS). 5FU was visualized using primary BrdU antibody (1:500 Sigma Aldrich) and the nucleolus was visualized by staining for nucleolin (1:1000 Cell signaling technology). Detection of primary antibodies was performed with Alexa Fluor 488 Goat anti-Mouse IgG (1:2000 Thermo Fisher Scientific) and Alexa Fluor 594 Goat anti-Rabbit IgG (1:2000 Thermo Fisher Scientific). Slides were mounted with Prolong Gold Antifade Mountant with DAPI (Thermo Fisher Scientific) and viewed using BZ-X710 fluorescence microscope or LSM700 confocal microscope (CLSM, Carl

bioRxiv preprint doi: https://doi.org/10.1101/2021.12.03.471189; this version posted December 9, 2021. The copyright holder for this preprint (which was not certified by peer review) is the author/funder. All rights reserved. No reuse allowed without permission.

Zeiss, Jena, Germany). For 5FU fluorescence quantification, three images were taken at random per treatment with a 100× objective lens and signal intensity was quantified from using ImageJ software. 5FU intensity for each image was divided by the number of cells and fold change was calculated by setting the control cells to one.

Cell line xenograft murine model

All animal care procedures were in accordance with institutional guidelines approved by the University of Tokyo. HCT116 cells (5×10^6 in 100 μL PBS) were inoculated subcutaneously in the right flank of nude mice. Established tumors (~110–120 mm^3) were randomized into vehicle, CX-5461 (50 mg/kg), or AMG 232 (50 mg/kg) treatment groups. Mice were treated with either oral gavage three times per week or i.p. administration as indicated. Tumor volume was measured by external caliper, and tumor volume was calculated using the formula (l × w2)/2, where w = width and l = length in mm of the tumor. Mouse body weight was measured three times per week. After treatments, animals were euthanized, and tumors were harvested for further analysis. Dissection of tumors to peripheral and core regions were performed according to a previous report[35].

Histological Analysis and Immunohistochemistry

Tumor tissues were fixed in 4% paraformaldehyde (PFA), embedded in paraffin, and subjected to hematoxylin and eosin (HE), periodic acid-Schiff (PAS) staining, and p53 staining.

bioRxiv preprint doi: https://doi.org/10.1101/2021.12.03.471189; this version posted December 9, 2021. The copyright holder for this preprint (which was not certified by peer review) is the author/funder. All rights reserved. No reuse allowed without permission.

Metabolite Extraction and Metabolome Analysis

Metabolites of tumor tissues were quantified in each sample using CE-MS (Agilent Technologies, Santa Clara, CA). To analyze cationic compounds, a fused silica capillary (50 mm i.d. 3 100 cm) was used with 1 M formic acid as the electrolyte. Methanol/water (50% v/v) containing 0.1 mM hexakis(2,2-difluoroethoxy)phosphazene was delivered as the sheath liquid at 10 mL/min. ESI-TOFMS was performed in positive ion mode, and the capillary voltage was set to 4 kV. Automatic recalibration of each acquired spectrum was achieved using the masses of the reference standards ([13C isotopic ion of a protonated methanol dimer (2 MeOH+H)]+, m/z 66.0632) and ([hexakis(2,2-difluoroethoxy)phosphazene +H]+, m/z 622.0290). To identify metabolites, relative migration times of all peaks were calculated by normalization to the reference compound 3-aminopyrrolidine. The metabolites were identified by comparing their m/z values and relative migration times to the metabolite standards. Quantification was performed by comparing peak areas to calibration curves generated using internal standardization techniques with methionine sulfone. To analyze anionic metabolites, a commercially available COSMO(+) (chemically coated with cationic polymer) capillary (50 mm i.d. x 105 cm) (Nacalai Tesque, Kyoto, Japan) was used with a 50 mM ammonium acetate solution (pH 8.5) as the electrolyte. Methanol/5 mM ammonium acetate (50% v/v) containing 0.1 mM hexakis(2,2-difluoroethoxy)phosphazene was delivered as the sheath liquid at 10 mL/min. ESI-TOFMS was performed in negative ion mode, and the capillary voltage was set to 3.5 kV. For anion analysis, trimesate and CAS were used as the reference and the internal standards, respectively. CE-TOFMS raw data were analyzed using

bioRxiv preprint doi: https://doi.org/10.1101/2021.12.03.471189; this version posted December 9, 2021. The copyright holder for this preprint (which was not certified by peer review) is the author/funder. All rights reserved. No reuse allowed without permission.

our proprietary software Master Hands (ver, 2.17.0.10). Briefly, the data processing for each experiment included data conversion, binning data into 0.02 m/z slices, baseline elimination, peak picking, integration, and elimination of redundant features to yield the all possible peaks lists. Data matrices were generated by an alignment process based on corrected migration times, and metabolite names were assigned to the aligned peaks by matching m/z and the corrected migration times of our standards library. Relative peak areas were calculated based on the ratio of peak area divided by those of internal standards, and metabolite concentrations were calculated based on the relative peak area between the sample and standard mixture.

Pulse-chase analysis

L-(methyl-^{3}H)-methionine pulse chase analysis was performed according to a previous report[49].

Polysomal profiling

Polysome profiling was performed as previously described[50] with some modifications. The cell lysate for polysome profiling was prepared as previously described[51] using lysis buffer (20 mM Tris, 15 mM $MgCl_2$, 300mM KCl, 0.5% NP40, 10 mM dithiothreitol, 100 units/mL RNasin, 100 mg/mL cycloheximide, protease and phosphatase inhibitors, pH 7.4). Sucrose density gradient (SDG) analysis was performed as previously described[52]. The lysate was layered on top of a sucrose gradient (10–50%, w/v) in the buffer (20 mM Tris, 100 mM KCl, 3 mM $MgCl_2$, pH 7.4) and separated by ultracentrifugation in a Beckman SW-41 Rotor at 36,000

bioRxiv preprint doi: https://doi.org/10.1101/2021.12.03.471189; this version posted December 9, 2021. The copyright holder for this preprint (which was not certified by peer review) is the author/funder. All rights reserved. No reuse allowed without permission.

rpm for 2 h 15 min at 4°C. Separated ribosomal subunits were fractionated using a Piston Gradient Fractionator (BIOCOMP), and the A260 was measured using an AC-5200 UV monitor (ATTO) and midi LOGGER GL840 (GRAPHTEC).

Statistical analysis

Plotted values are shown as mean ± standard deviation throughout this study. Indicated P values are expressed as: n.s. non-significant, *$p < 0.05$, **$p < 0.01$, ***$p < 0.001$. Student's two-tailed T test was used to calculate statistical significance.

Author Contributions

M. P. designed the study; M.P., C.Z., K.I., M.S., M.K., M.N., A.O., T. Soga, T.O. performed experiments; H.Z., M.C., H.A., J.S., Y.M., T. Suzuki, advised on critical experiments; M.P., D.L., C.G.P. wrote the manuscript.

Acknowledgements

We thank the members of the Laboratory for Systems Biology and Medicine and Integrative Nutriomics and Oncology, RCAST, the University of Tokyo. We especially thank Dr. Shintaro Iwasaki and Dr. T. Tanaka for helpful discussions. This work was supported by Grant-in-Aid for Scientific Research B (19H03496, T.O.), Scientific Research on Innovative Areas (20H04834, T.O.) and Grant-in-Aid for challenging Exploratory Research (19K22553, T.O.) from the Ministry of Education, Culture, Sports, Science and Technology of Japan, The Tokyo Biochemical Research Foundation (T.O.), Life Science Foundation of Japan (T.O.), Princess Takamatsu Cancer research Found (T.O.), The Naito Foundation (T.O.), The Uehara Memorial

bioRxiv preprint doi: https://doi.org/10.1101/2021.12.03.471189; this version posted December 9, 2021. The copyright holder for this preprint (which was not certified by peer review) is the author/funder. All rights reserved. No reuse allowed without permission.

Foundation (T.O.). JetPub Scientific Communications, LLC provided editorial assistance to the authors during preparation of this manuscript.

Competing Interests

Authors declare no competing interests.

bioRxiv preprint doi: https://doi.org/10.1101/2021.12.03.471189; this version posted December 9, 2021. The copyright holder for this preprint (which was not certified by peer review) is the author/funder. All rights reserved. No reuse allowed without permission.

References

1. El-Naggar, A. M. *et al.* Translational Activation of HIF1α by YB-1 Promotes Sarcoma Metastasis. *Cancer Cell* **27**, (2015).
2. Leprivier, G. *et al.* The eEF2 kinase confers resistance to nutrient deprivation by blocking translation elongation. *Cell* **153**, 1064–1079 (2013).
3. Thomlinson, R. H. & Gray, L. H. The histological structure of some human lung cancers and the possible implications for radiotherapy. *Br. J. Cancer* **9**, 539–549 (1955).
4. Dewhirst, M. W. A potential solution for eliminating hypoxia as a cause for radioresistance. *Proceedings of the National Academy of Sciences of the United States of America* vol. 115 10548–10550 (2018).
5. Kimura, H. *et al.* Fluctuations in red cell flux in tumor microvessels can lead to transient hypoxia and reoxygenation in tumor parenchyma. *Cancer Res.* **56**, 5522–5528 (1996).
6. Harris, A. L. Hypoxia--a key regulatory factor in tumour growth. *Nat. Rev. Cancer* **2**, 38–47 (2002).
7. Jones, R. G. & Thompson, C. B. Tumor suppressors and cell metabolism: a recipe for cancer growth. *Genes Dev.* **23**, 537–548 (2009).
8. Pàez-Ribes, M. *et al.* Antiangiogenic therapy elicits malignant progression of tumors to increased local invasion and distant metastasis. *Cancer Cell* **15**, 220–231 (2009).
9. Osawa, T. & Shibuya, M. Targeting cancer cells resistant to hypoxia and nutrient starvation to improve anti-angiogeneic therapy. *Cell cycle* vol. 12 2519–2520 (2013).
10. Silvera, D., Formenti, S. C. & Schneider, R. J. Translational control in cancer. *Nature Reviews Cancer* vol. 10 254–266 (2010).
11. El-Naggar, A. M. & Sorensen, P. H. Translational control of aberrant stress responses as a hallmark of cancer. *J. Pathol.* **244**, 650–666 (2018).
12. Buttgereit, F. & Brand, M. D. A hierarchy of ATP-consuming processes in mammalian

bioRxiv preprint doi: https://doi.org/10.1101/2021.12.03.471189; this version posted December 9, 2021. The copyright holder for this preprint (which was not certified by peer review) is the author/funder. All rights reserved. No reuse allowed without permission.

cells. *Biochem. J* **312 (Pt 1)**, 163–167 (1995).

13. Liu, G. Y. & Sabatini, D. M. mTOR at the nexus of nutrition, growth, ageing and disease. *Nat. Rev. Mol. Cell Biol.* **21**, 183–203 (2020).
14. Costa-Mattioli, M. & Walter, P. The integrated stress response: From mechanism to disease. *Science* **368**, (2020).
15. Mayer, C., Zhao, J., Yuan, X. & Grummt, I. mTOR-dependent activation of the transcription factor TIF-IA links rRNA synthesis to nutrient availability. *Genes Dev.* **18**, 423–434 (2004).
16. Hoppe, S. *et al.* AMP-activated protein kinase adapts rRNA synthesis to cellular energy supply. *Proc. Natl. Acad. Sci. U. S. A.* **106**, 17781–17786 (2009).
17. Lafontaine, D. L. J. Noncoding RNAs in eukaryotic ribosome biogenesis and function. *Nat. Struct. Mol. Biol.* **22**, 11–19 (2015).
18. Bohnsack, K. E. & Bohnsack, M. T. Uncovering the assembly pathway of human ribosomes and its emerging links to disease. *EMBO J.* **38**, e100278 (2019).
19. Tafforeau, L. *et al.* The complexity of human ribosome biogenesis revealed by systematic nucleolar screening of Pre-rRNA processing factors. *Mol. Cell* **51**, 539–551 (2013).
20. Aubert, M., O'Donohue, M.-F., Lebaron, S. & Gleizes, P.-E. Pre-Ribosomal RNA Processing in Human Cells: From Mechanisms to Congenital Diseases. *Biomolecules* **8**, (2018).
21. Levine, A. J. p53: 800 million years of evolution and 40 years of discovery. *Nat. Rev. Cancer* **20**, 471–480 (2020).
22. Sloan, K. E., Bohnsack, M. T. & Watkins, N. J. The 5S RNP couples p53 homeostasis to ribosome biogenesis and nucleolar stress. *Cell Rep.* **5**, 237–247 (2013).
23. Donati, G., Peddigari, S., Mercer, C. A. & Thomas, G. 5S ribosomal RNA is an essential component of a nascent ribosomal precursor complex that regulates the Hdm2-p53

bioRxiv preprint doi: https://doi.org/10.1101/2021.12.03.471189; this version posted December 9, 2021. The copyright holder for this preprint (which was not certified by peer review) is the author/funder. All rights reserved. No reuse allowed without permission.

checkpoint. *Cell Rep.* **4**, 87–98 (2013).

24. Nicolas, E. *et al.* Involvement of human ribosomal proteins in nucleolar structure and p53-dependent nucleolar stress. *Nat. Commun.* **7**, 11390 (2016).
25. Bywater, M. J. *et al.* Inhibition of RNA polymerase I as a therapeutic strategy to promote cancer-specific activation of p53. *Cancer Cell* **22**, 51–65 (2012).
26. Peltonen, K. *et al.* A targeting modality for destruction of RNA polymerase I that possesses anticancer activity. *Cancer Cell* **25**, 77–90 (2014).
27. Devlin, J. R. *et al.* Combination Therapy Targeting Ribosome Biogenesis and mRNA Translation Synergistically Extends Survival in MYC-Driven Lymphoma. *Cancer Discov.* **6**, 59–70 (2016).
28. Hein, N. *et al.* Inhibition of Pol I transcription treats murine and human AML by targeting the leukemia-initiating cell population. *Blood* vol. 129 2882–2895 (2017).
29. Khot, A. *et al.* First-in-Human RNA Polymerase I Transcription Inhibitor CX-5461 in Patients with Advanced Hematologic Cancers: Results of a Phase I Dose-Escalation Study. *Cancer Discov.* **9**, 1036–1049 (2019).
30. Drygin, D. *et al.* Targeting RNA polymerase I with an oral small molecule CX-5461 inhibits ribosomal RNA synthesis and solid tumor growth. *Cancer Res.* **71**, 1418–1430 (2011).
31. Pestov, D. G., Lapik, Y. R. & Lau, L. F. Assays for ribosomal RNA processing and ribosome assembly. *Curr. Protoc. Cell Biol.* **Chapter 22**, Unit 22.11 (2008).
32. Popov, A. *et al.* Duration of the first steps of the human rRNA processing. *Nucleus* **4**, 134–141 (2013).
33. Boulon, S., Westman, B. J., Hutten, S., Boisvert, F.-M. & Lamond, A. I. The Nucleolus under Stress. *Molecular Cell* vol. 40 216–227 (2010).
34. Kalita, K., Makonchuk, D., Gomes, C., Zheng, J.-J. & Hetman, M. Inhibition of nucleolar transcription as a trigger for neuronal apoptosis. *J. Neurochem.* **105**, 2286–2299 (2008).

bioRxiv preprint doi: https://doi.org/10.1101/2021.12.03.471189; this version posted December 9, 2021. The copyright holder for this preprint (which was not certified by peer review) is the author/funder. All rights reserved. No reuse allowed without permission.

35. Pan, M. *et al.* Regional glutamine deficiency in tumours promotes dedifferentiation through inhibition of histone demethylation. *Nat. Cell Biol.* **18**, 1090–1101 (2016).

36. Bursać, S. *et al.* Mutual protection of ribosomal proteins L5 and L11 from degradation is essential for p53 activation upon ribosomal biogenesis stress. *Proc. Natl. Acad. Sci. U. S. A.* **109**, 20467–20472 (2012).

37. Sun, X.-X., Wang, Y.-G., Xirodimas, D. P. & Dai, M.-S. Perturbation of 60 S ribosomal biogenesis results in ribosomal protein L5- and L11-dependent p53 activation. *J. Biol. Chem.* **285**, 25812–25821 (2010).

38. Fumagalli, S., Ivanenkov, V. V., Teng, T. & Thomas, G. Suprainduction of p53 by disruption of 40S and 60S ribosome biogenesis leads to the activation of a novel G2/M checkpoint. *Genes Dev.* **26**, 1028–1040 (2012).

39. Fumagalli, S. *et al.* Absence of nucleolar disruption after impairment of 40S ribosome biogenesis reveals an rpL11-translation-dependent mechanism of p53 induction. *Nat. Cell Biol.* **11**, 501–508 (2009).

40. Durán, R. V. *et al.* Glutaminolysis activates Rag-mTORC1 signaling. *Mol. Cell* **47**, 349–358 (2012).

41. Villar, V. H. *et al.* mTORC1 inhibition in cancer cells protects from glutaminolysis-mediated apoptosis during nutrient limitation. *Nat. Commun.* **8**, 14124 (2017).

42. Mamane, Y., Petroulakis, E., LeBacquer, O. & Sonenberg, N. mTOR, translation initiation and cancer. *Oncogene* **25**, 6416–6422 (2006).

43. Eukaryotic Elongation Factor 2 Kinase (eEF2K) in Cancer. *Cancers* **9**, (2017).

44. Wang, X. *et al.* Eukaryotic elongation factor 2 kinase activity is controlled by multiple inputs from oncogenic signaling. *Mol. Cell. Biol.* **34**, 4088–4103 (2014).

45. Thoreen, C. C. *et al.* A unifying model for mTORC1-mediated regulation of mRNA translation. *Nature* **485**, 109–113 (2012).

bioRxiv preprint doi: https://doi.org/10.1101/2021.12.03.471189; this version posted December 9, 2021. The copyright holder for this preprint (which was not certified by peer review) is the author/funder. All rights reserved. No reuse allowed without permission.

46. Iadevaia, V., Liu, R. & Proud, C. G. mTORC1 signaling controls multiple steps in ribosome biogenesis. *Semin. Cell Dev. Biol.* **36**, 113–120 (2014).

47. Xu, H. *et al.* CX-5461 is a DNA G-quadruplex stabilizer with selective lethality in BRCA1/2 deficient tumours. *Nat. Commun.* **8**, 14432 (2017).

48. Wernerman, J. Clinical use of glutamine supplementation. *J. Nutr.* **138**, 2040S–2044S (2008).

49. Zorbas, C. *et al.* The human 18S rRNA base methyltransferases DIMT1L and WBSCR22-TRMT112 but not rRNA modification are required for ribosome biogenesis. *Molecular Biology of the Cell* vol. 26 2080–2095 (2015).

50. Õunap, K., Käsper, L., Kurg, A. & Kurg, R. The human WBSCR22 protein is involved in the biogenesis of the 40S ribosomal subunits in mammalian cells. *PLoS One* **8**, e75686 (2013).

51. Mohammad, F. & Buskirk, A. Protocol for Ribosome Profiling in Bacteria. *BIO-PROTOCOL* vol. 9 (2019).

52. Ishiguro, K., Arai, T. & Suzuki, T. Depletion of S-adenosylmethionine impacts on ribosome biogenesis through hypomodification of a single rRNA methylation. *Nucleic Acids Res.* **47**, 4226–4239 (2019).

bioRxiv preprint doi: https://doi.org/10.1101/2021.12.03.471189; this version posted December 9, 2021. The copyright holder for this preprint (which was not certified by peer review) is the author/funder. All rights reserved. No reuse allowed without permission.

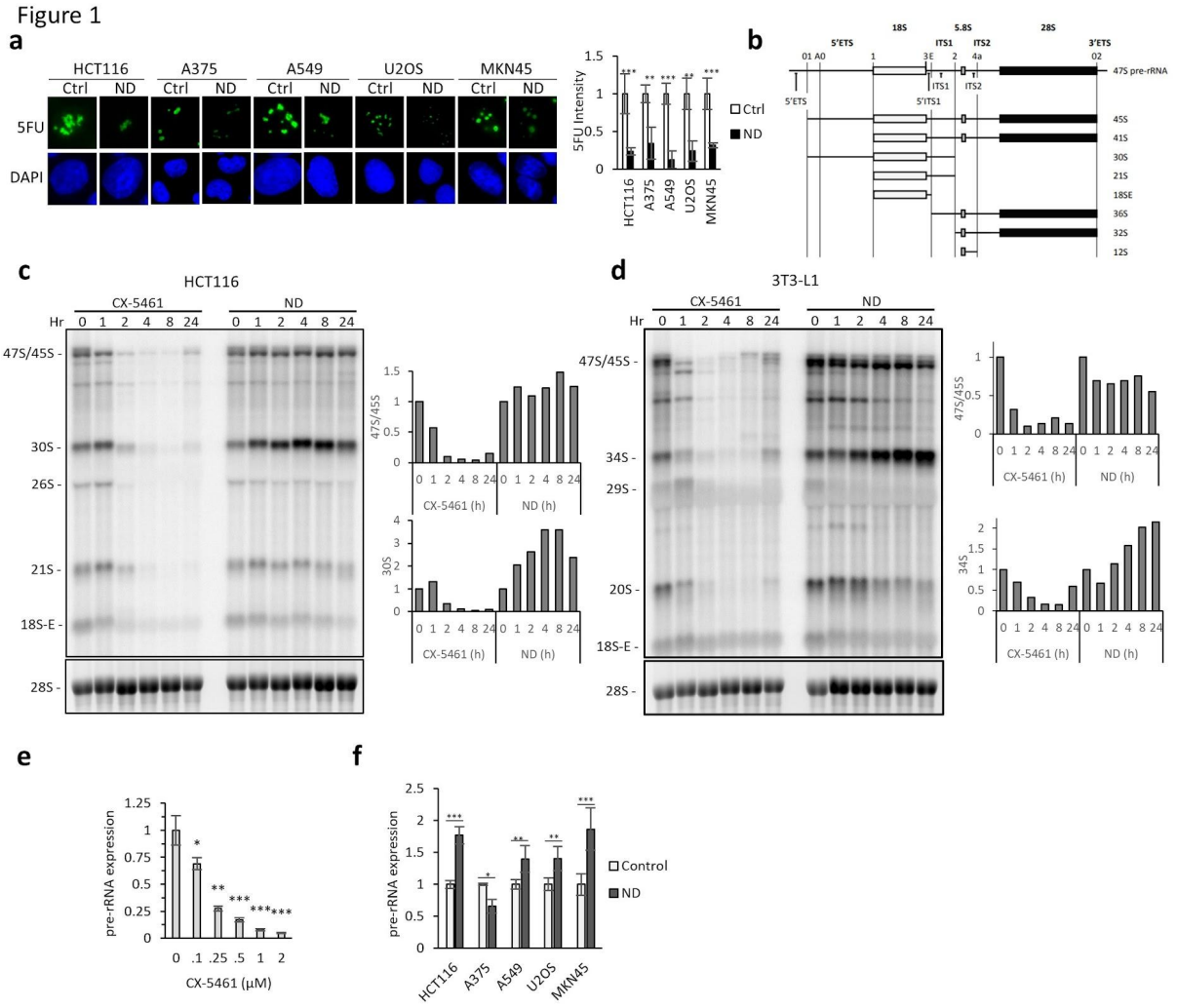

Figure 1: Nutrient deprivation upregulates pre-rRNA expression

(a) 5FU labelling under nutrient deprivation (24 h). Cancer cell lines were cultured under ND (-Glucose –Amino acids –FBS) for 24 h, and pre-rRNA synthesis was measured by 5FU metabolic labelling.

(b) Schematic of pre-rRNA processing. 47S processing produces intermediate precursors which mature to 18S, 28S, and 5.8S rRNAs. The primary 47S pre-rRNA contains two external transcribed spacers (5'ETS and 3'ETS) and two internal transcriber spacers (ITS1 and ITS2).

(c) Left: Pre-rRNA expression in HCT116 treated to CX-5461 or ND using northern blotting (ITS1 Probe). Right: Quantification of 47S/45S and 30S intermediates in response to CX-5461/ND. The full northern blot is shown in Supplementary Fig. 1b.

(d) Left: Pre-rRNA expression in 3T3-L1 cells treated to CX-5461 or ND using northern blotting (ITS1 Probe). Right: Quantification of 47S/45S and 34S intermediates in response to CX-5461/ND. The full northern blot is shown in Supplementary Fig. 1c.

(e) Expression of pre-rRNAs (47S/45S/30S species) after CX-5461 (8 h) exposure.

(f) Expression of pre-rRNAs (47S/45S/30S species) after 24 h ND in HCT116, A549, U2OS, and MKN45 cells, as assessed using qRT-PCR.

bioRxiv preprint doi: https://doi.org/10.1101/2021.12.03.471189; this version posted December 9, 2021. The copyright holder for this preprint (which was not certified by peer review) is the author/funder. All rights reserved. No reuse allowed without permission.

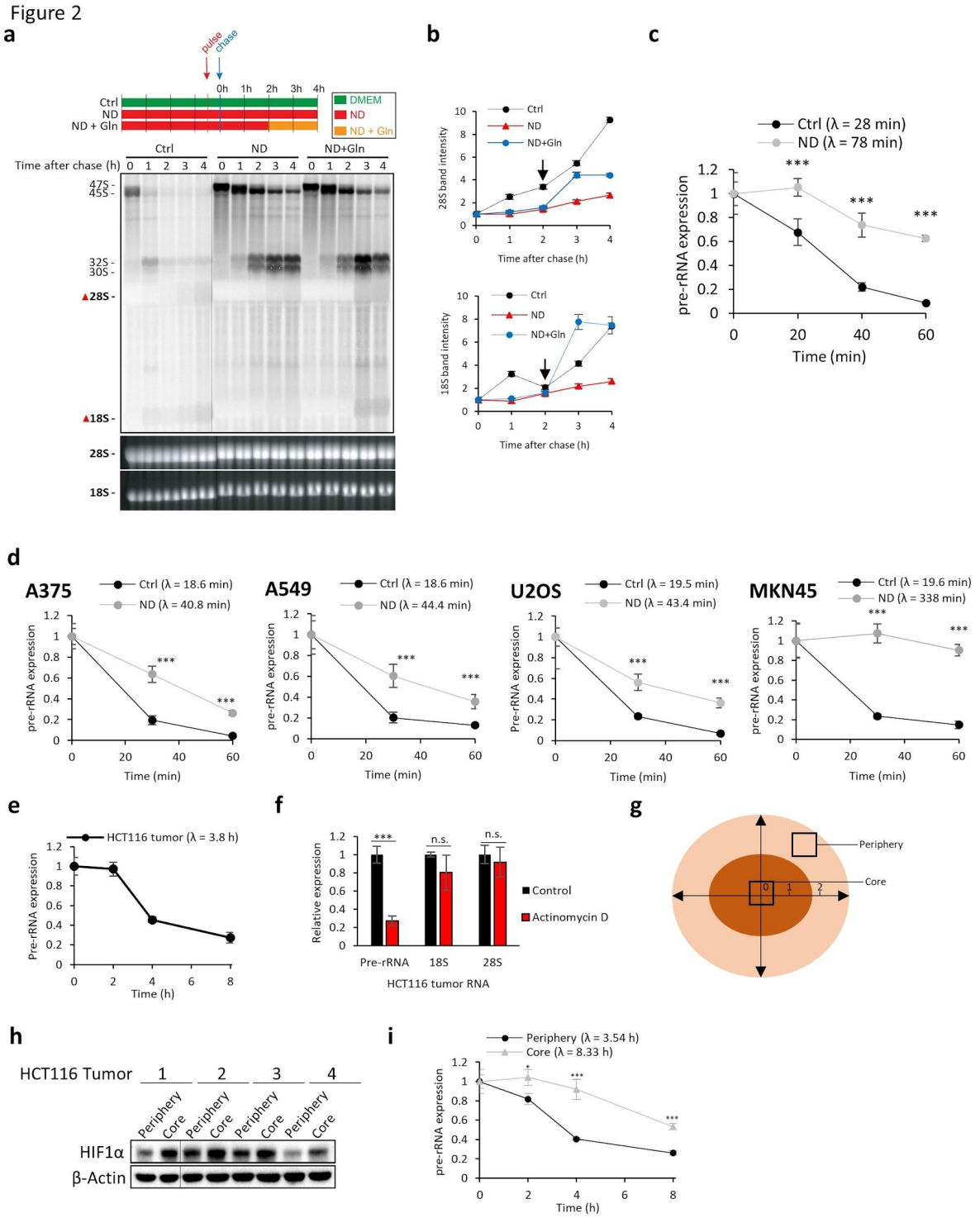

Figure 2: Pre-rRNA processing is impaired under ND

(a) Analysis of pre-rRNA processing kinetics in control or ND HCT116 cells. HCT116 cells that were pre-treated to 3.5 hr ND were subsequently pulse labeled with L-(methyl-3H)-methionine for 30 min and chased with excess cold methionine. To assess the effect of nutrient restoration on pre-rRNAs accumulated under ND, Gln was added back to the ND medium 2 h after the cold methionine chase ("ND+Gln"). To quantify mature rRNA production, the intensity of the 18S/28S bands (indicated by the red triangles) were quantified (Fig. 2b).

bioRxiv preprint doi: https://doi.org/10.1101/2021.12.03.471189; this version posted December 9, 2021. The copyright holder for this preprint (which was not certified by peer review) is the author/funder. All rights reserved. No reuse allowed without permission.

(b) Quantification of the 28S/18S bands from Fig 1f (as indicated by the red triangles). The black arrow at the 2 hour time point indicates the time at which glutamine was added to starved (ND) cells.
(c) ND increases the pre-rRNA half-life (λ) as assessed using qRT-PCR. HCT116 cells were pretreated to (24 h) ND, transcription was stopped by (20 μM) actinomycin D, and total RNA at the indicated time points for qRT-PCR analysis. The pre-rRNA half-life was approximated using linear regression.
(d) ND slows pre-rRNA processing and increases the pre-rRNA half-life (λ) as assessed using qRT-PCR. Cancer cells were pretreated to ND (24 h), transcription was stopped by ActD (20 μM) treatment, and total RNA was collected from cell lysates at the indicated time points. Half-life was approximated using linear regression
(e) HCT116 tumor pre-rRNA (47S, 45S, 30S species) half-life as determined using qRT-PCR. Actinomycin D (1.33 mM) was intratumorally injected into established HCT116 tumors; tissue from the injection site was collected for RNA extraction at the indicated time points.
(f) Expression of pre-rRNAs, 18S, and 28S in HCT116 tumors after actinomycin D (1.33 mM) intratumoral injection. (n.s.: not significant)
(g) Schematic of core and periphery regions of established HCT116 tumors (approximate size 1000 mm^3). One unit equals 33% of the radius.
(h) Expression of HIF1α in HCT116 periphery and core tissues as assessed using western blotting.
(i) Pre-rRNA processing is faster in peripheral tissues compared to core tissues, as determined using qRT-PCR. Actinomycin D (1.33 mM) was intratumorally injected into established HCT116 tumors and dissected into periphery and core samples at the indicated time points for RNA extraction. Each time point represents periphery and core tissues dissected from the same tumor.

bioRxiv preprint doi: https://doi.org/10.1101/2021.12.03.471189; this version posted December 9, 2021. The copyright holder for this preprint (which was not certified by peer review) is the author/funder. All rights reserved. No reuse allowed without permission.

Figure 3

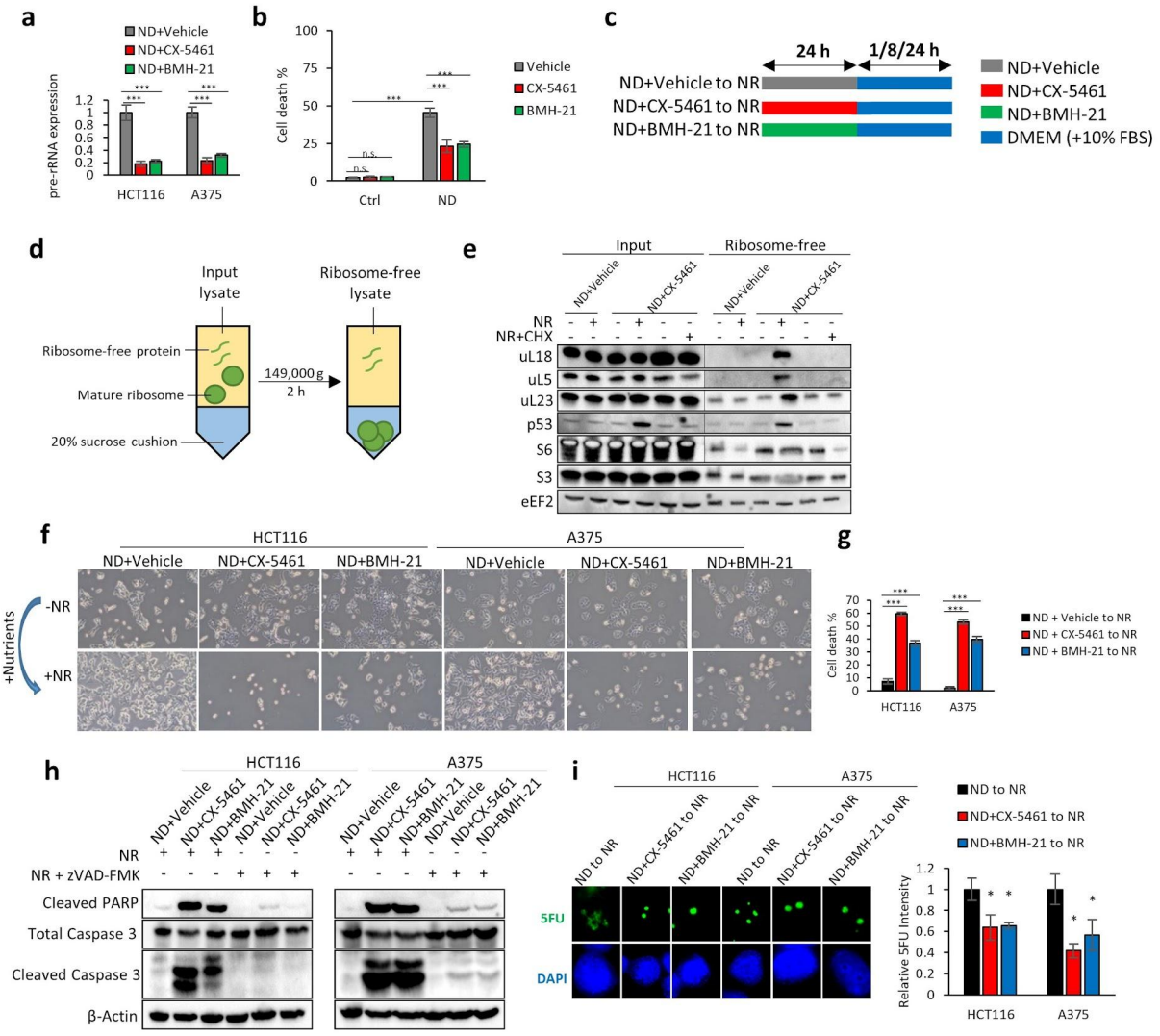

Figure 3: Pre-rRNA accumulation is an adaptive response to nutrient restoration

(a) Pre-rRNA expression in HCT116 and A375 cells after treatment with vehicle (NaH2PO4), CX-5461 (10 μM), or BMH-21 (1 μM) under 24 h ND. Graph show mean values±st. dev. (n=3).

(b) Percentage of cell death in HCT116 cells cultured in control or ND medium with vehicle (NaH2PO4), CX-5461 (10 μM), or BMH-21 (1 μM) as assessed using trypan blue exclusion assay. Graph show mean values±st. dev. (n=3). (n.s.: not significant)

(c) Schematic showing ND and nutrient restoration (NR) treatments. To inhibit pre-rRNA expression, HCT116 or A375 cells were first placed under ND in the presence of vehicle (NaH2PO4), CX-5461 (10 μM), or BMH-21 (1 μM). After 24 h, RNA was isolated and assessed for pre-rRNA expression using qRT-PCR. Cells pre-treated to ND+CX-5461/ND+BMH-21 represent “pre-rRNA-depleted” cells. To induce metabolic recovery, pre-starved cells (ND+Vehicle/ND+CX-5461/ND+BMH-21) were washed three times with PBS and were allowed to rest in drug-free DMEM (10% FBS)

bioRxiv preprint doi: https://doi.org/10.1101/2021.12.03.471189; this version posted December 9, 2021. The copyright holder for this preprint (which was not certified by peer review) is the author/funder. All rights reserved. No reuse allowed without permission.

(d) In order to assess the expression of ribosome-free proteins, input lysates were clarified of large ribosomes using sucrose cushion ultracentrifugation (149,000 g 2 h). The resulting ribosome-free lysates were analyzed using western blotting.
(e) Expression of ribosome-free r-proteins in metabolically recovering HCT116 cells. HCT116 were incubated with vehicle (NaH2PO4) or CX-5461 (10 μM) under ND for 24 h; after 24 h, the treatment medium was replaced with DMEM (NR) or DMEM plus cycloheximide (NR+CHX) for 8 h.
(f) NR induces cell death in pre-rRNA-depleted HCT116 and A375 cells. HCT116 and A375 cells were treated with CX-5461 (10 μM) or BMH-21 (1 μM) to inhibit pre-rRNA expression under ND; after 24 h, the treatment medium was replaced with a drug-free basal medium (DMEM 10% FBS). Representative microscopy images were taken after 24 h of NR.
(g) Percentage of cell death of metabolically recovering HCT116 or A375 cells, as determined using trypan blue exclusion assay (n = 3).
(h) NR induces caspase 3 and PARP cleavage in pre-rRNA HCT116 and A375 cells, which is inhibited by the pan-caspase inhibitor zVAD-FMK (1 μM). HCT116 and A375 cells under ND were co-treated with vehicle (NaH2PO4), CX-5461 (10 μM), or BMH-21 (1 μM); after 24 h the treatment media was replaced with a basal medium containing DMSO or zVAD-FMK (1 μM). Protein lysates were collected after 24 h NR for western blotting.
(i) Pre-rRNA synthesis resumes after CX-5461/BMH-21 drug washout and NR. HCT116 and A375 cells were cultured in ND medium in the presence of Vehicle, CX-5461 (10 μM), or BMH-21 (1 μM). After 24 h, the cells were washed three times with PBS and were allowed to rest in DMEM for 24 h. The rate of pre-rRNA synthesis by Pol I was measured using the 5-Fluorouridine (5FU) labelling assay.

bioRxiv preprint doi: https://doi.org/10.1101/2021.12.03.471189; this version posted December 9, 2021. The copyright holder for this preprint (which was not certified by peer review) is the author/funder. All rights reserved. No reuse allowed without permission.

Figure 4

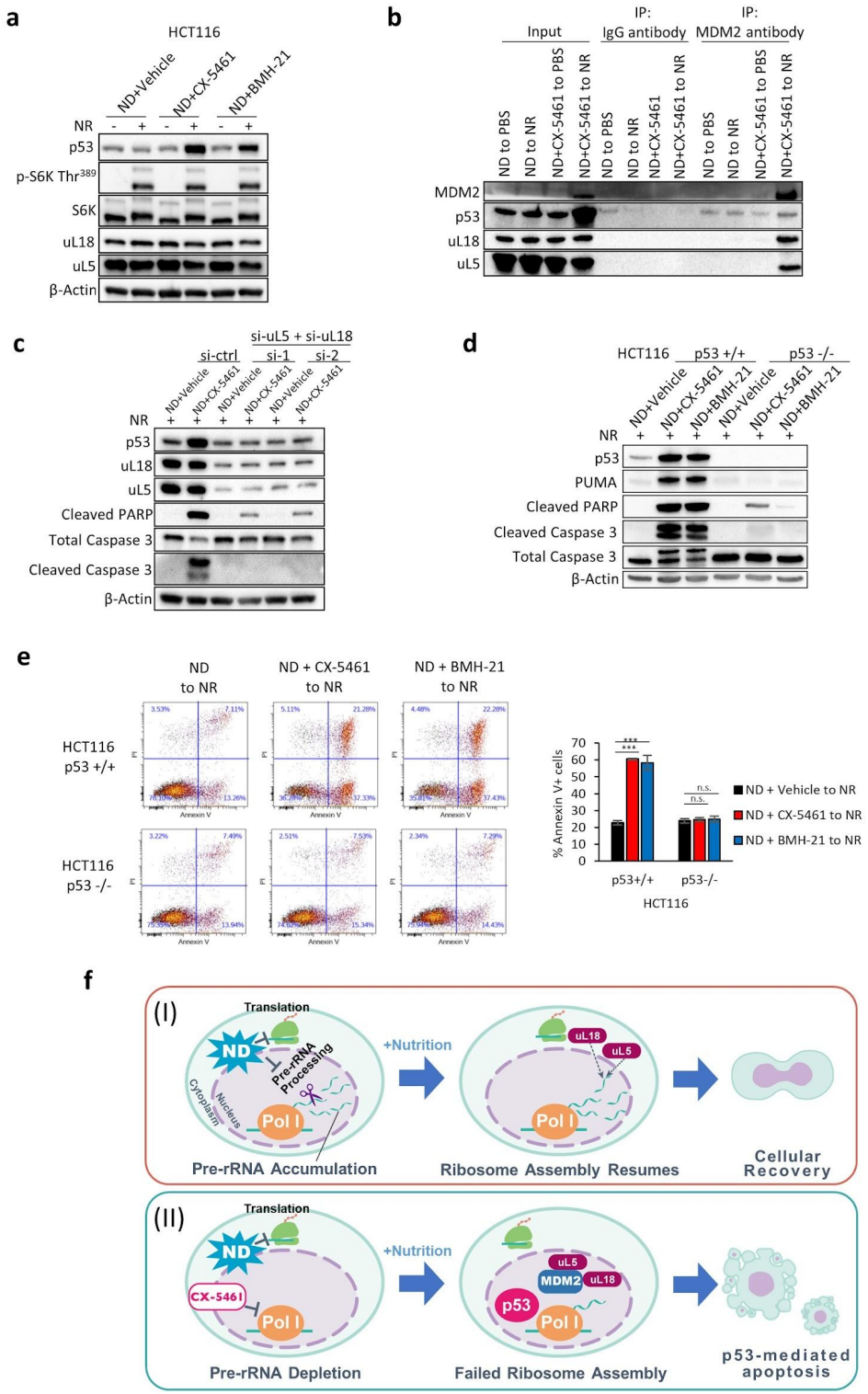

Figure 4: Nucleolar surveillance drives NR-mediated apoptosis

(a) NR induces p53 in pre-rRNA depleted HCT116 cells as assessed using western blotting. HCT116 cells were cultured in ND medium with vehicle (NaH2PO4), CX-5461 (10 μM), or BMH-21 (1 μM) for 24 h; after 24 h, the treatment medium was replaced with a drug-free basal medium (NR) for 8 h.

(b) Co-immunoprecipitation of p53, uL5, and uL18 with MDM2. HCT116 cells were

bioRxiv preprint doi: https://doi.org/10.1101/2021.12.03.471189; this version posted December 9, 2021. The copyright holder for this preprint (which was not certified by peer review) is the author/funder. All rights reserved. No reuse allowed without permission.

cultured under ND with vehicle (NaH2PO4) or CX-5461 (10 μM) for 24 h; after 24 h, cells were treated to PBS or NR for 12 h.
(c) Dual knockdown of uL5 and uL18 by siRNA inhibits NR-mediated activation of p53 and apoptotic markers. HCT116 cells were transfected with control or two different sets of siRNAs targeting uL5 and uL18. After 48 h, cells were placed under ND with CX-5461 (10 μM) for 24 h. After 24 h, the treatment medium was replaced with a drug-free basal medium for 8 h and the protein lysate was collected for western blotting.
(d) NR induces apoptosis in HCT116 p53 +/+ cells but not p53 -/- cells. HCT116 p53 +/+ or p53 -/- cells were incubated under ND with vehicle (NaH2PO4), CX-5461 (10 μM), or BMH-21 (1 μM) for 24 h; after 24 h, the treatment medium was replaced with a drug-free basal medium for 24 h and the protein lysate was collected for western blotting.
(e) NR induces apoptosis in pre-rRNA depleted HCT116 p53+/+ cells but not HCT116 p53-/- cells, as determined using Annexin V-PI flow cytometry. (n.s.: not significant)
(f) (I) pre-rRNA intermediates accumulate in nutrient deprived cancer cells. In parallel, ND suppresses global mRNA translation. Following nutrient addition (NR), accumulated pre-rRNAs are bound by newly translated uL5 and uL18 for ribosome assembly. (II) Treatment with CX-5461 prevents cancer cells from accumulating pre-rRNAs under ND. Following NR, upon the absence of endogenous pre-rRNAs, uL5 and uL18 binds to MDM2, leading to p53 stabilization and nutrient-induced apoptosis.

bioRxiv preprint doi: https://doi.org/10.1101/2021.12.03.471189; this version posted December 9, 2021. The copyright holder for this preprint (which was not certified by peer review) is the author/funder. All rights reserved. No reuse allowed without permission.

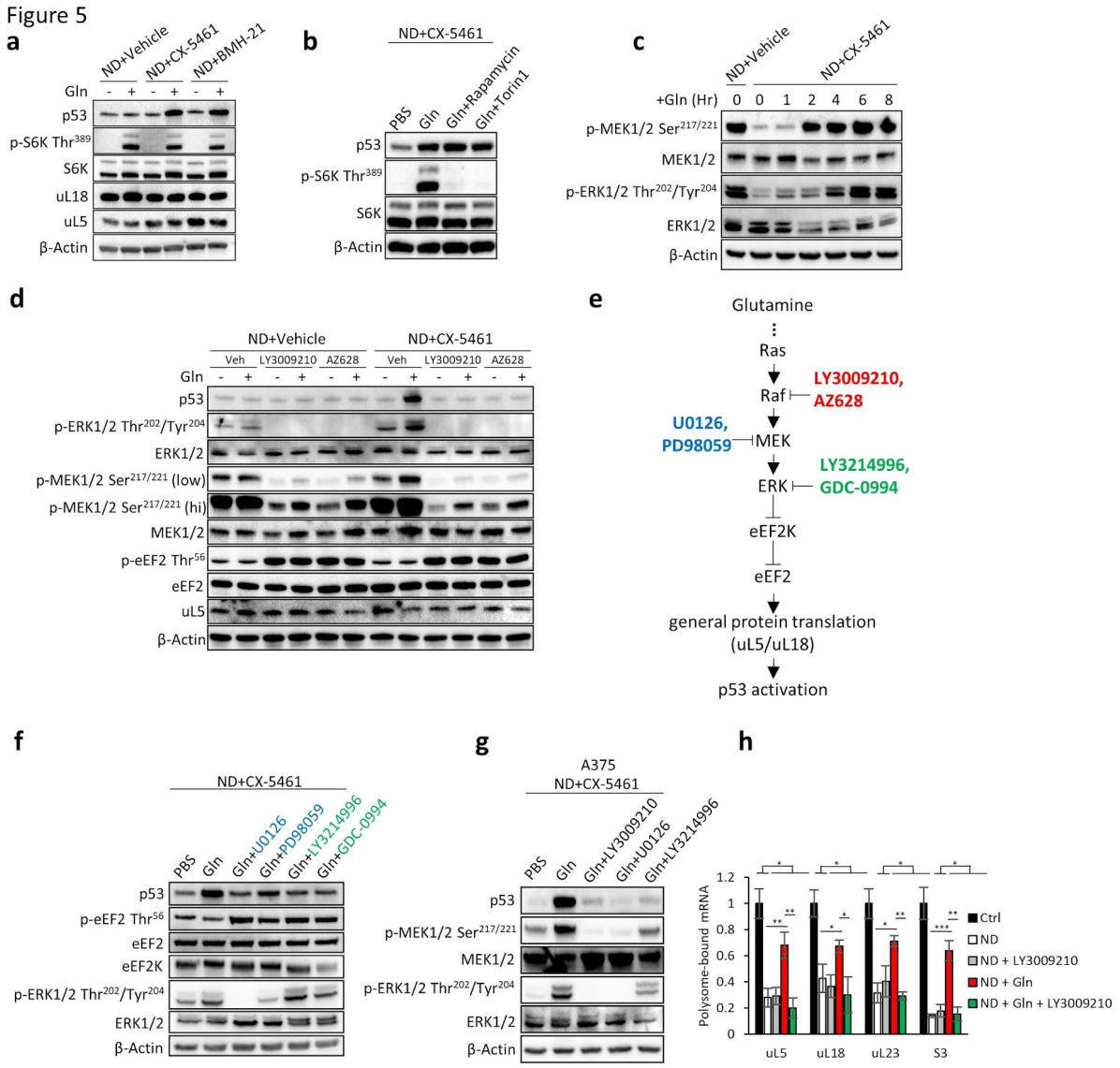

Figure 5: Glutamine metabolically activates p53 by inducing uL5/uL18 translation

(a) Glutamine (gln) activates p53 in pre-rRNA depleted HCT116 cells as assessed by western blotting. HCT116 were cultured in ND medium with vehicle (NaH_2PO_4), CX-5461 (10 μM), or BMH-21 (1 μM) for 24 h. After 24 h the old treatment media was replaced with ND media containing PBS or Gln (4 mM) for 8 h.

(b) Inhibiting mTORC1 with Rapamycin (1 μM) or Torin1 (1 μM) does not decrease the stabilization of p53 by glutamine.

(c) Glutamine restoration rescues MEK and ERK phosphorylation in pre-rRNA-depleted A375 cells. A375 cells were cultured in ND media in the presence of CX-5461 (10 μM). After 24 h, 4 mM gln was added back to the starvation media for the indicated time points.

(d) Inhibiting Raf with LY3009210 (400 nM) or AZ628 (500 nM) inhibits the metabolic activation of p53 by glutamine (gln). HCT116 cells were placed under ND with CX-5461 (10 μM) for 24 h. After 24 h the old treatment media was replaced with ND media containing PBS, Gln (4 mM), or Gln (4mM) with LY3009210/AZ628.

bioRxiv preprint doi: https://doi.org/10.1101/2021.12.03.471189; this version posted December 9, 2021. The copyright holder for this preprint (which was not certified by peer review) is the author/funder. All rights reserved. No reuse allowed without permission.

(e) Schematic: Glutamine restoration activates Ras/Raf/MEK/ERK signaling, which inhibits eEF2K. Upon eEF2K inhibition, eEF2 remains in its active form to facilitate global protein synthesis (including uL5/uL18 translation). Pharmacological inhibition of Raf/MEK/ERK leads to eEF2k activation, which in turn phosphorylates and inactivates eEF2.
(f) Inhibiting MEK (10 μM U0126, 50 μM PD98059) or ERK (1 μM LY3214996, 0.1 μM GDC-0994) inhibits the metabolic activation of p53 by glutamine (gln). HCT116 cells were placed under ND with CX-5461 (10 μM) for 24 h. After 24 h the old treatment media was replaced with ND media containing PBS, Gln (4 mM), or Gln (4mM) with U0126/PD98059/LY3214996/GDC-0994.
(g) Inhibiting Raf (400 nM LY3009210), MEK (10 μM U0126) and ERK (1 μM LY3214996) inhibits the metabolic activation of p53 by glutamine (gln) in A375 cells. A375 cells were placed under ND with CX-5461 (10 μM) for 24 h. After 24 h the old treatment media was replaced with ND media containing PBS, Gln (4 mM), or Gln (4mM) with drug.
(h) Expression of polysome-bound r-protein mRNAs. HCT116 cells were placed under ND for 24 h. After 24 h the old treatment media was replaced with ND media containing 4 mM Gln, LY3009210 (400 nM), or Gln + LY3009210. Polysomes were collected via ultracentrifugation on a 40% sucrose cushion and total RNA was extracted and assayed using qRT-PCR for uL5, uL18, uL23, and S3.

bioRxiv preprint doi: https://doi.org/10.1101/2021.12.03.471189; this version posted December 9, 2021. The copyright holder for this preprint (which was not certified by peer review) is the author/funder. All rights reserved. No reuse allowed without permission.

Figure 6

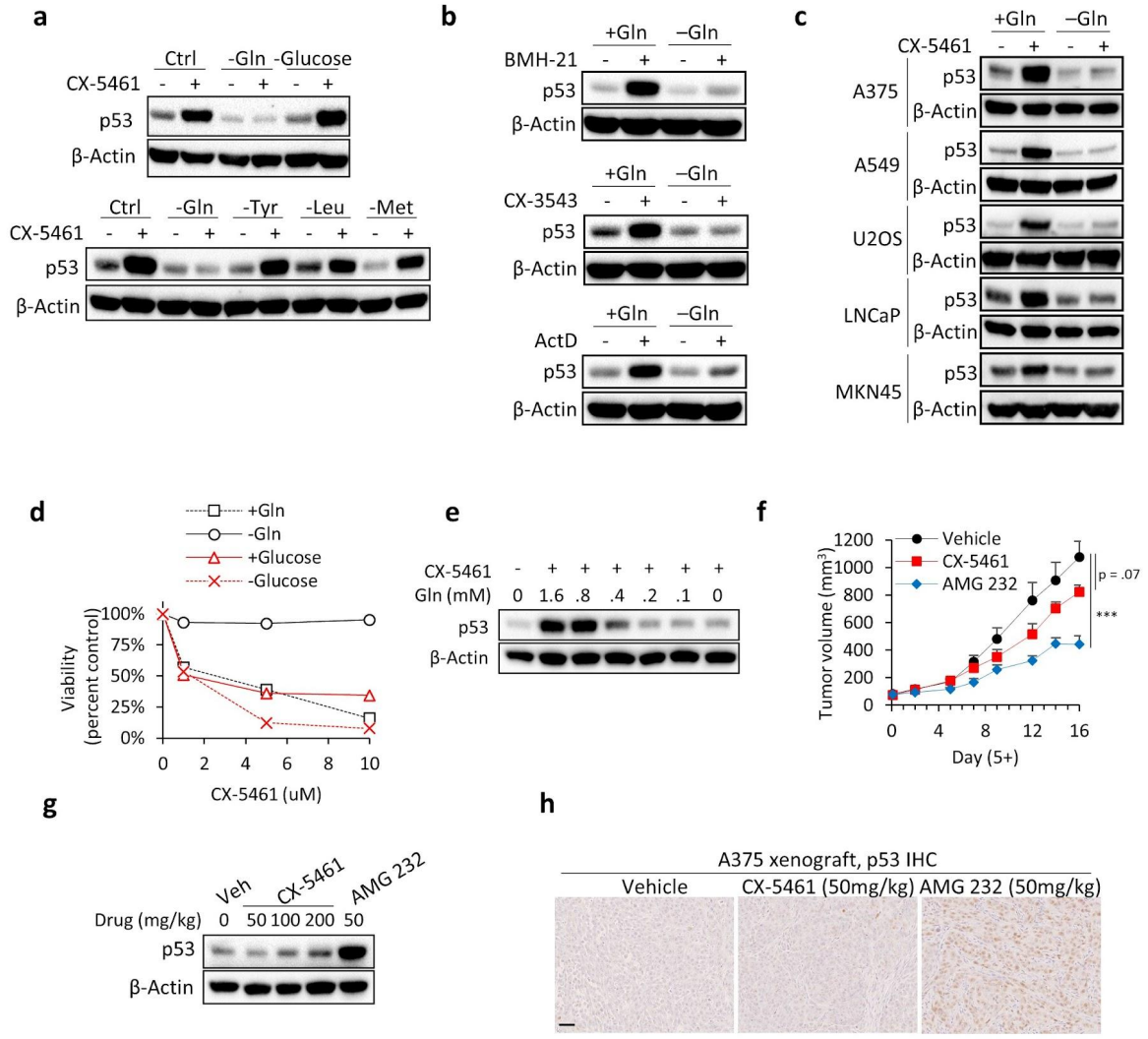

Figure 6: Glutamine deprivation confers cancer cells resistance to RNA Pol I inhibitors by blocking the nucleolar surveillance pathway

(a) Glutamine deprivation inhibits the activation of p53 by CX-5461 treatment. HCT116 cells were cultured in the respective starvation medium for 16 h followed by CX-5461 (1 μM) for 8 h.

(b) Glutamine deprivation inhibits p53 activation by BMH-21, CX-3543, and ActD as assessed by western blotting. HCT116 cells were cultured in +Gln or -Gln conditions for 16 h followed by treatment with BMH-21 (0.1 μM), CX-3543 (1 μM), or ActD (1 nM) for 8 h.

(c) Glutamine deprivation inhibits p53 activation by CX-5461 (1 μM) in A375, A549, U2OS, LNCaP, and MKN45 cells.

(d) Deprivation of glutamine but not glucose conferred resistance to CX-5461 as assessed using MTT assay. HCT116 cells were incubated in the respective control or starvation medium with vehicle (NaH_2PO_4) or CX-5461 at the indicated concentrations for 72 h. Data points of each treatment was normalized to the respective vehicle-treated metabolic control.

(e) p53 activation by CX-5461 was suppressed under 0.4 mM glutamine as assessed

bioRxiv preprint doi: https://doi.org/10.1101/2021.12.03.471189; this version posted December 9, 2021. The copyright holder for this preprint (which was not certified by peer review) is the author/funder. All rights reserved. No reuse allowed without permission.

by western blotting. HCT116 cells were cultured in the respective starvation medium for 16 h followed by CX-5461 (1 μM) for 8 h.
(f) CX-5461 failed to inhibit HCT116 tumor growth. Mice were orally dosed with vehicle (NaH2PO4), CX-5461 (50 mg/kg), or AMG 232 (50 mg/kg) once daily three times per week. Drug treatment started 5 days post-implantation on tumors of approximately 75 mm3. Each point is the mean tumor volume ± stdev (n = 8/group).
(g) CX-5461 does not acutely stabilize p53 in HCT116 tumors. Mice were IP injected with vehicle (NaH2PO4), CX-5461 (50, 100, 200 mg/kg), or AMG 232 (50 mg/kg) and tumors were harvested after 8 h for western blot analysis.
(h) p53 IHC staining in A375 tumors. Mice were IP injected with vehicle (NaH2PO4), CX-5461 (50 mg/kg), or AMG 232 (50 mg/kg), and tumors were harvested 16 h later for IHC. Scale bar represents 50 μm.